Highlights

1. Lens capsule integrity is essential but not the only requirement for regeneration
2. LECs sense their local environment to select an EMT or regeneration response
3. Cell proliferation, repolarisation and cell loss are early post-surgery responses
4. Bag in the Lens and Lens in the Bag both produce similar Soemmerring's Rings (SR)
5. SR formation and functional lens regeneration are different endpoints

Figure 1

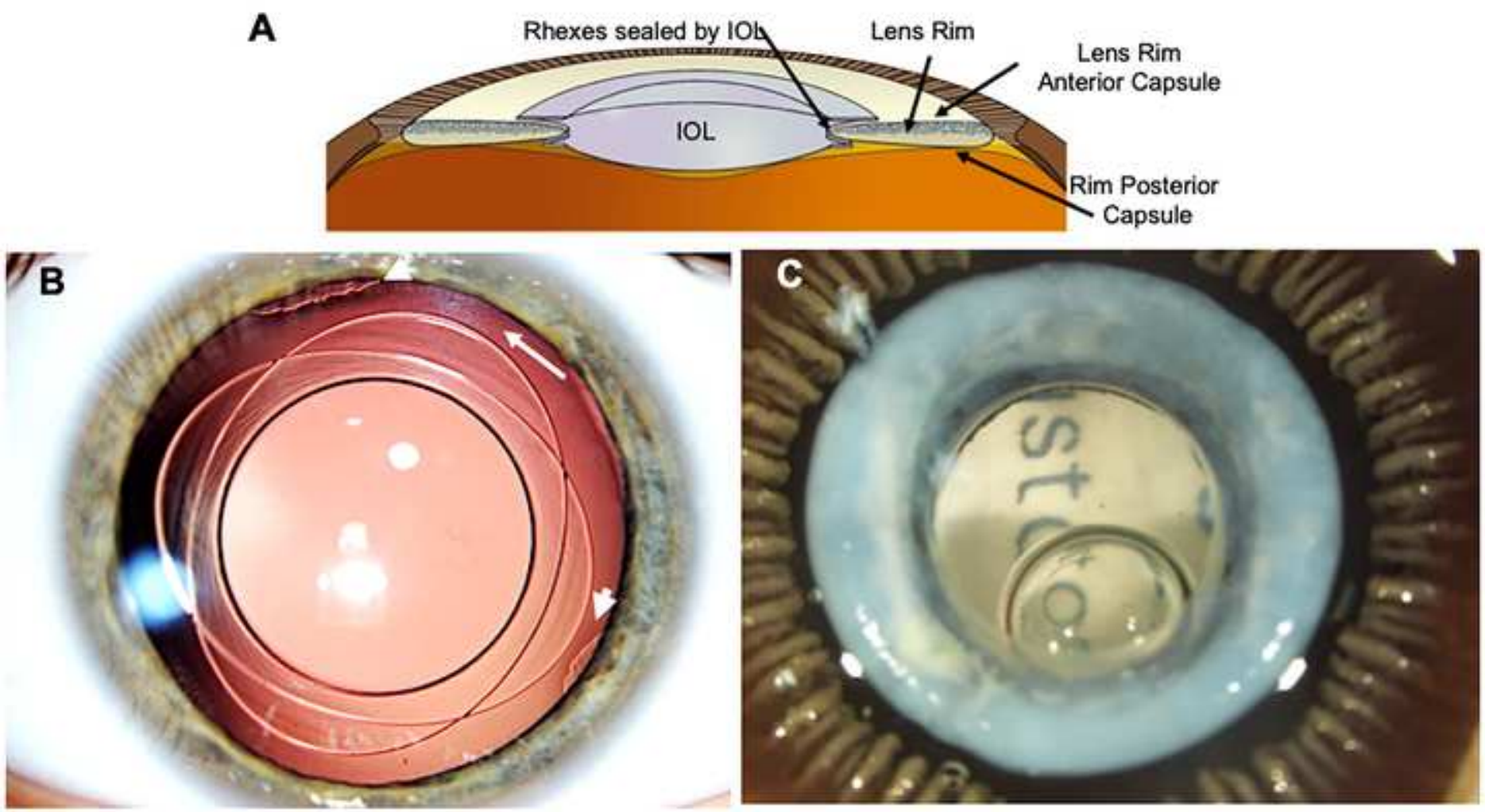

Figure 1. Wu et al

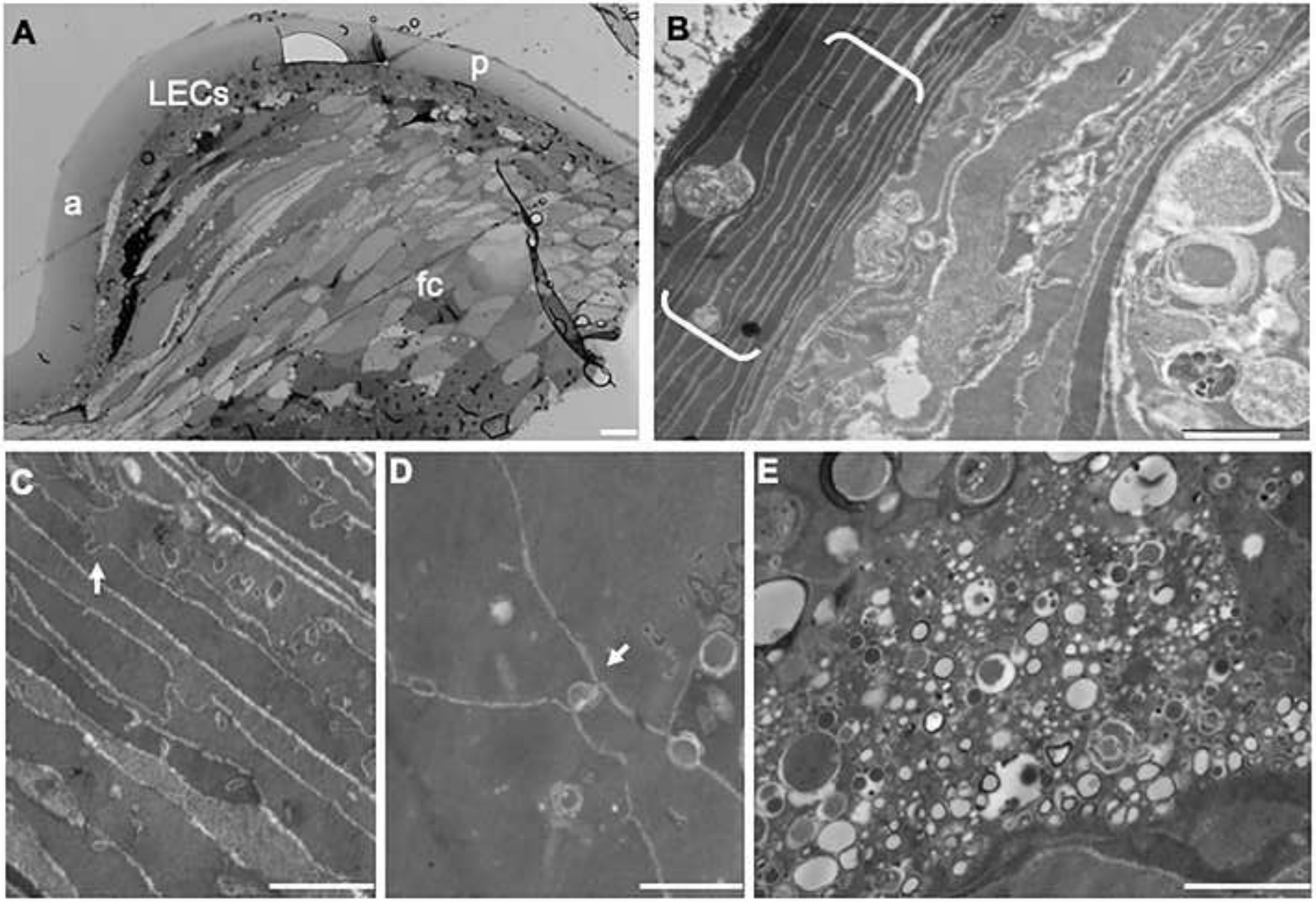

Figure 2. Wu et al

Figure 2F

Click here to access/download;Figure;Figure2F.tif

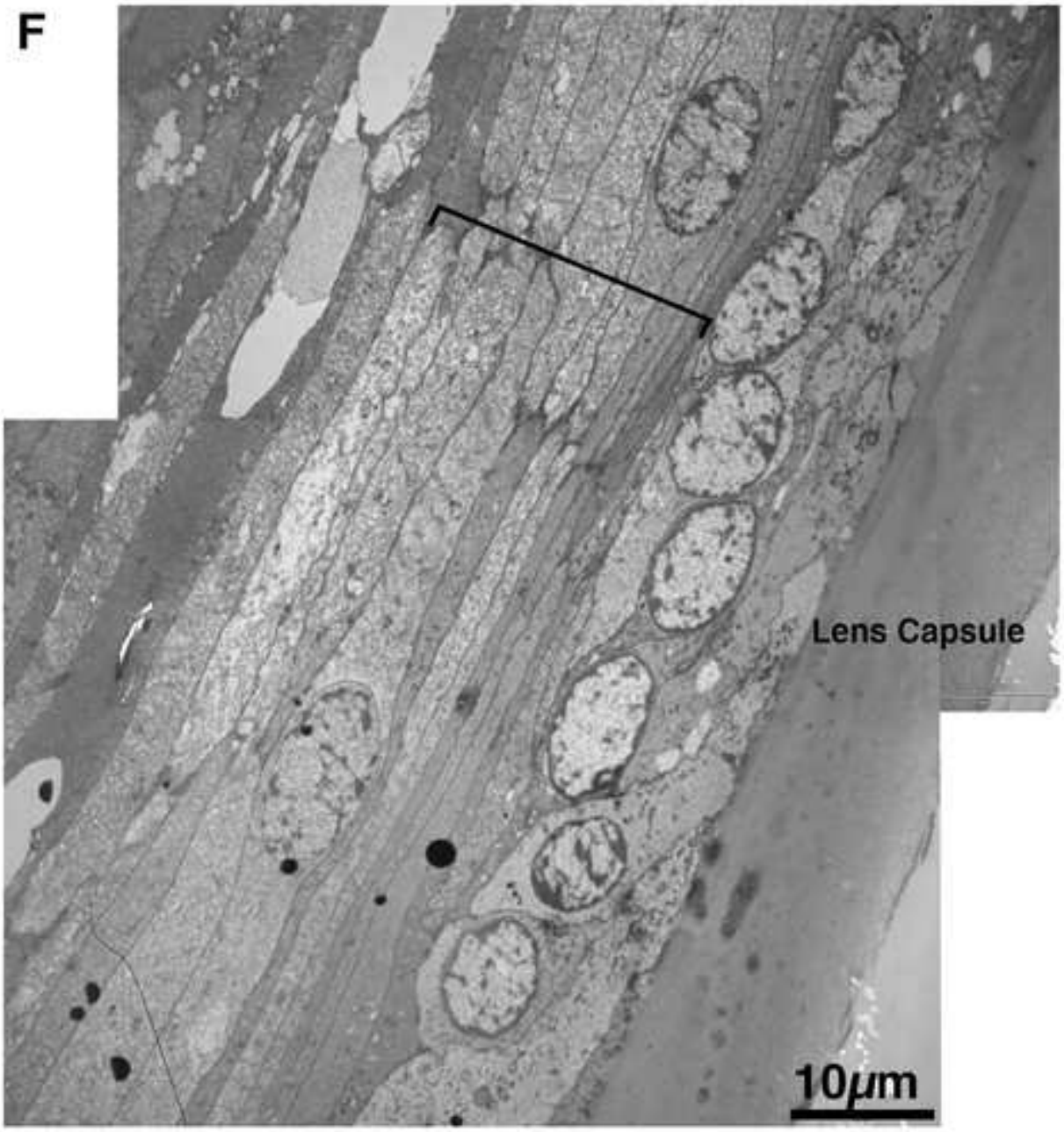

Figure 2F

Figure 3

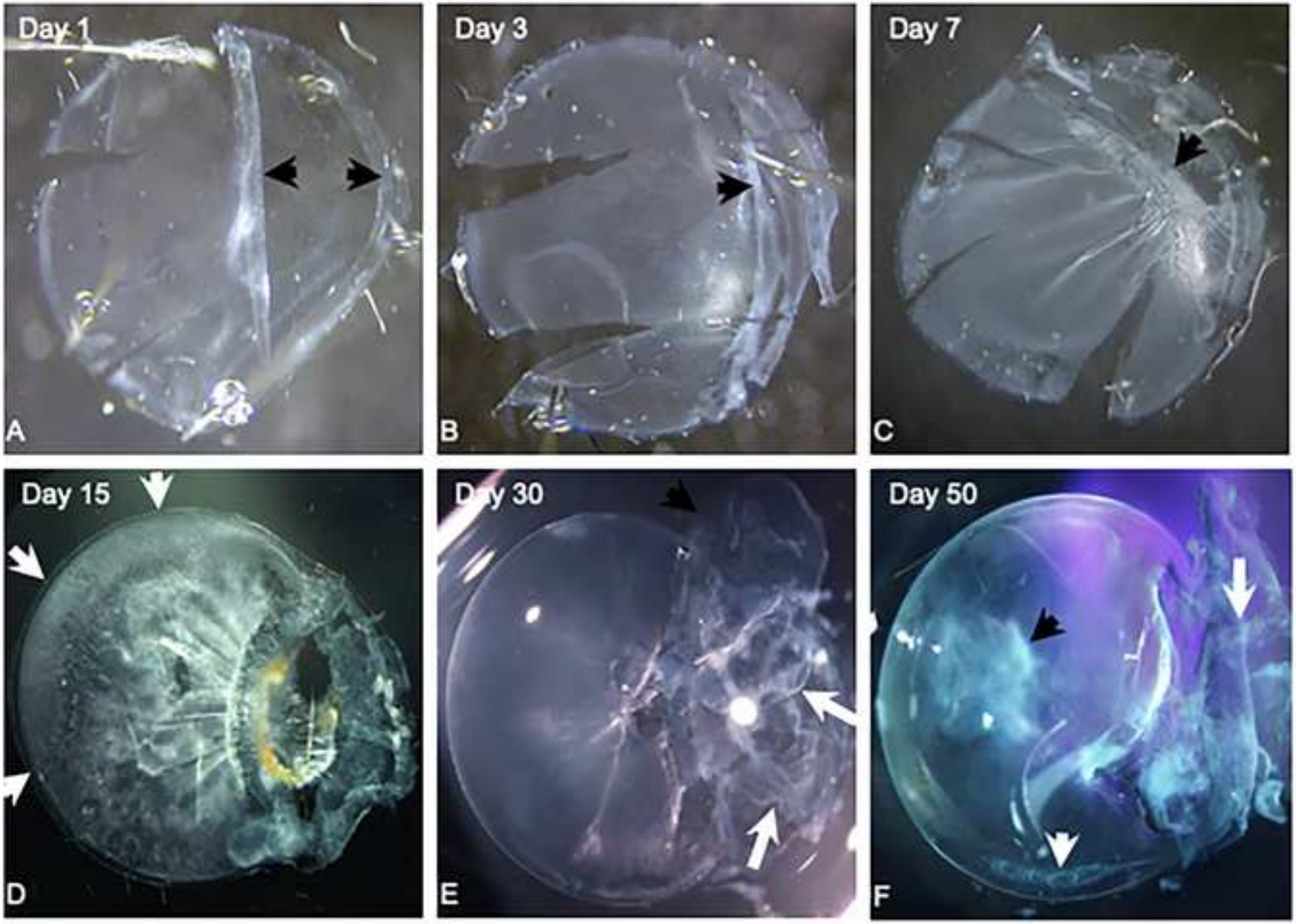

Figure 3. Wu et al

Figure 4A,B

Click here to access/download;Figure;Fig4A,Bnew.tif

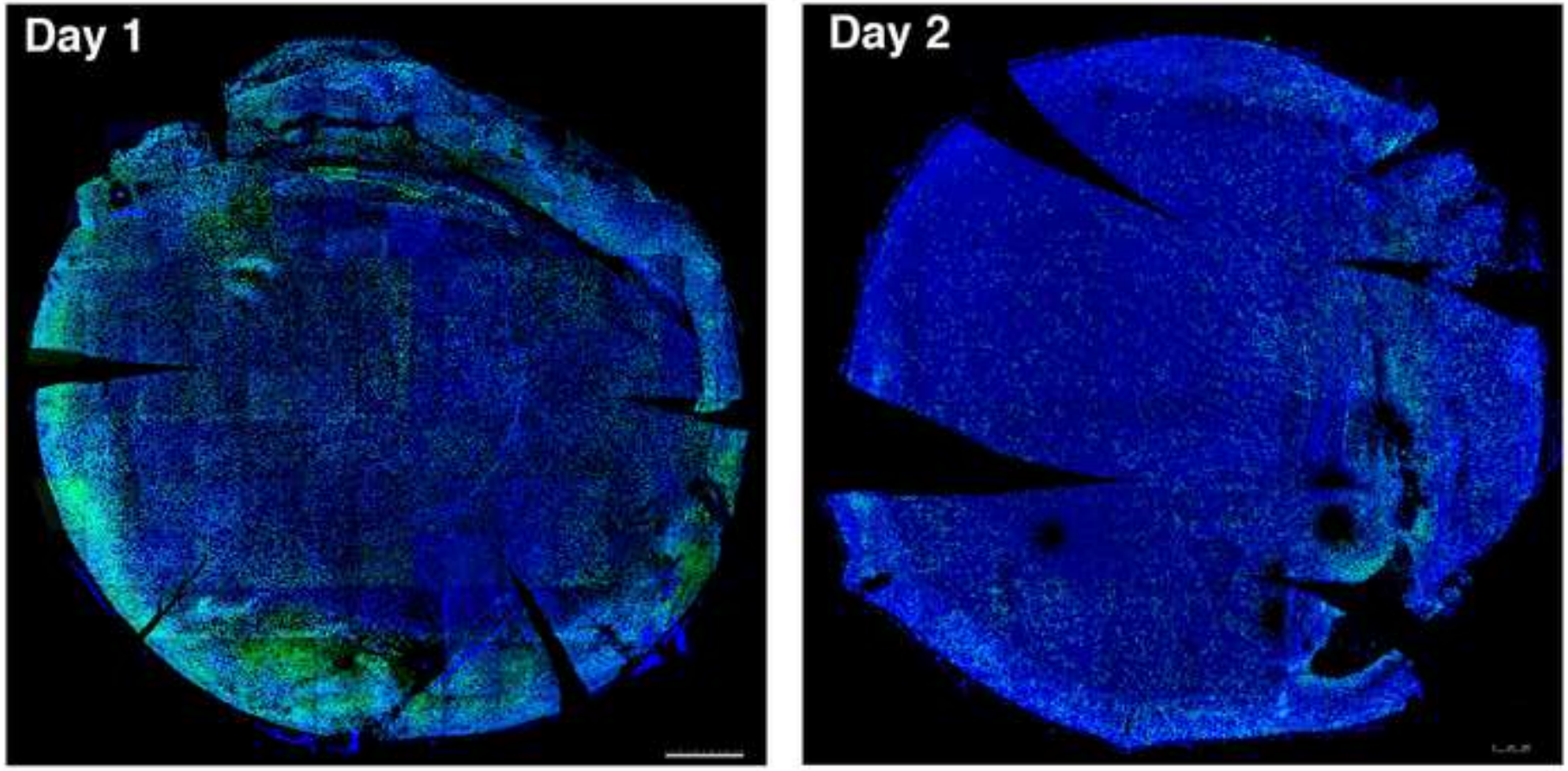

Figure 4C

Click here to access/download;Figure;Figure4C_WuEER21.tif

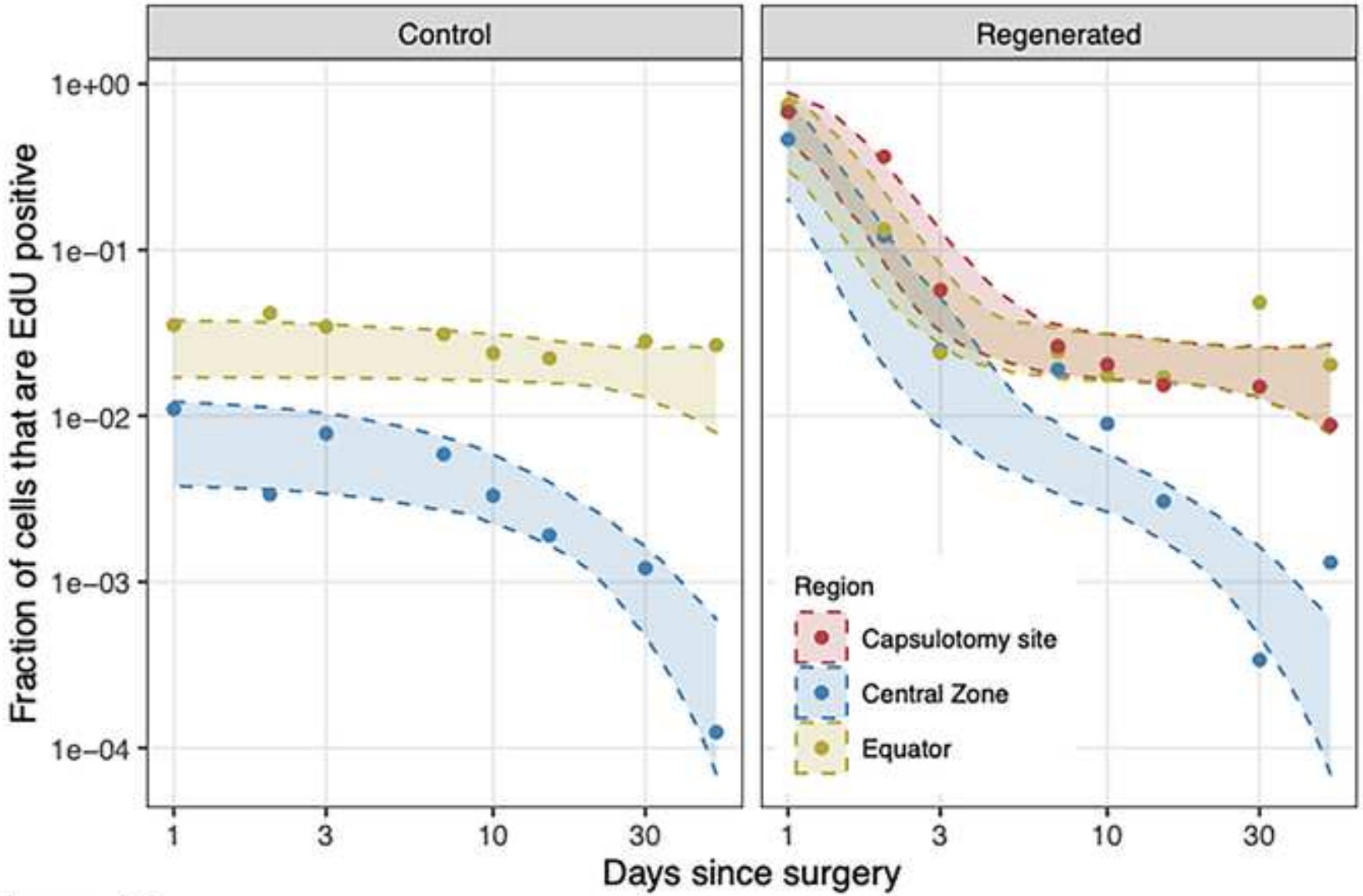

Figure 4C

Figure 5

Click here to access/download;Figure;Figure5_WuEER21_600dpi.tif

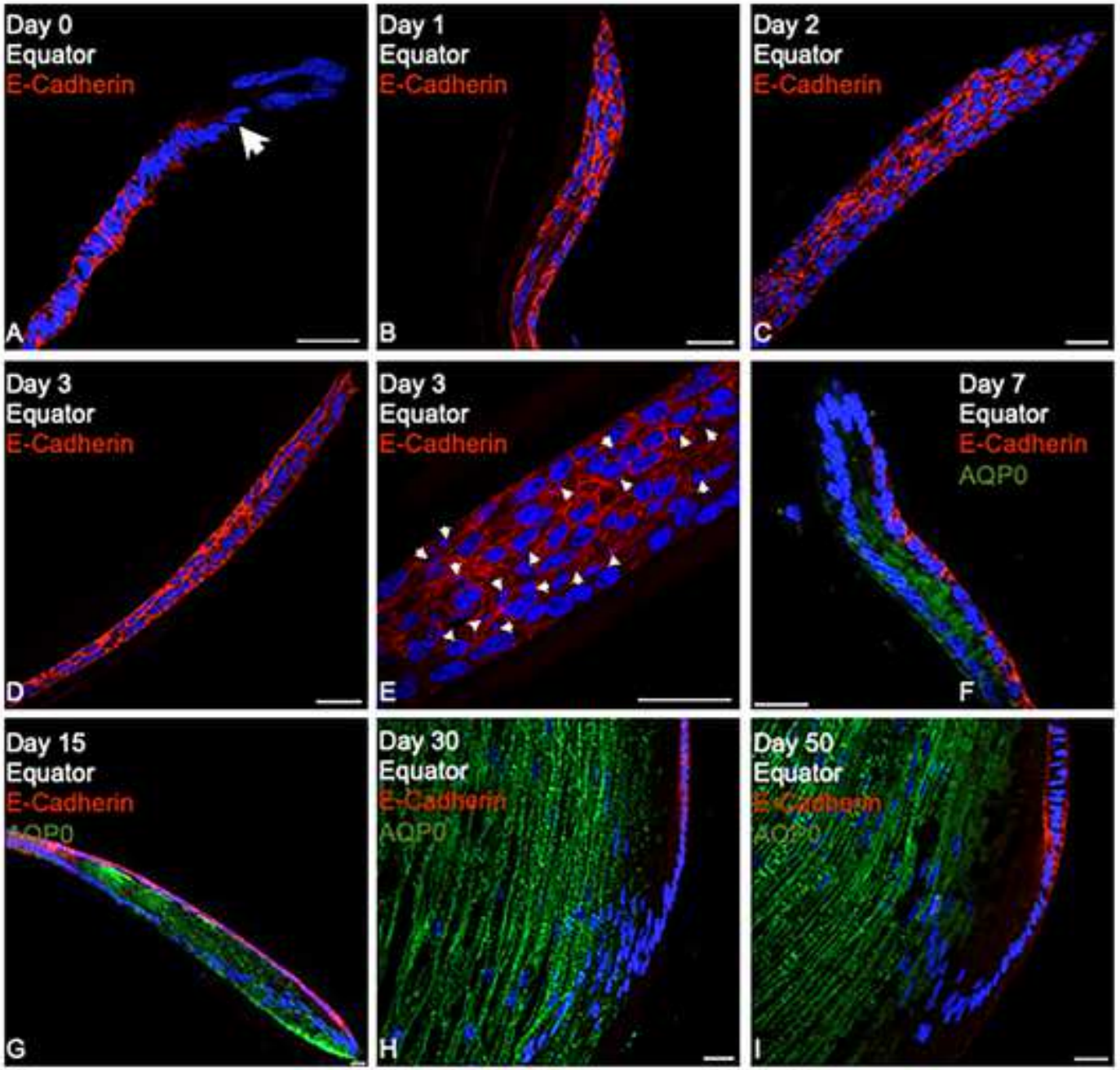

Figure 5. Wu et al

Figure 6

Click here to access/download;Figure;Figure6_WuEER21_600dpi.tif

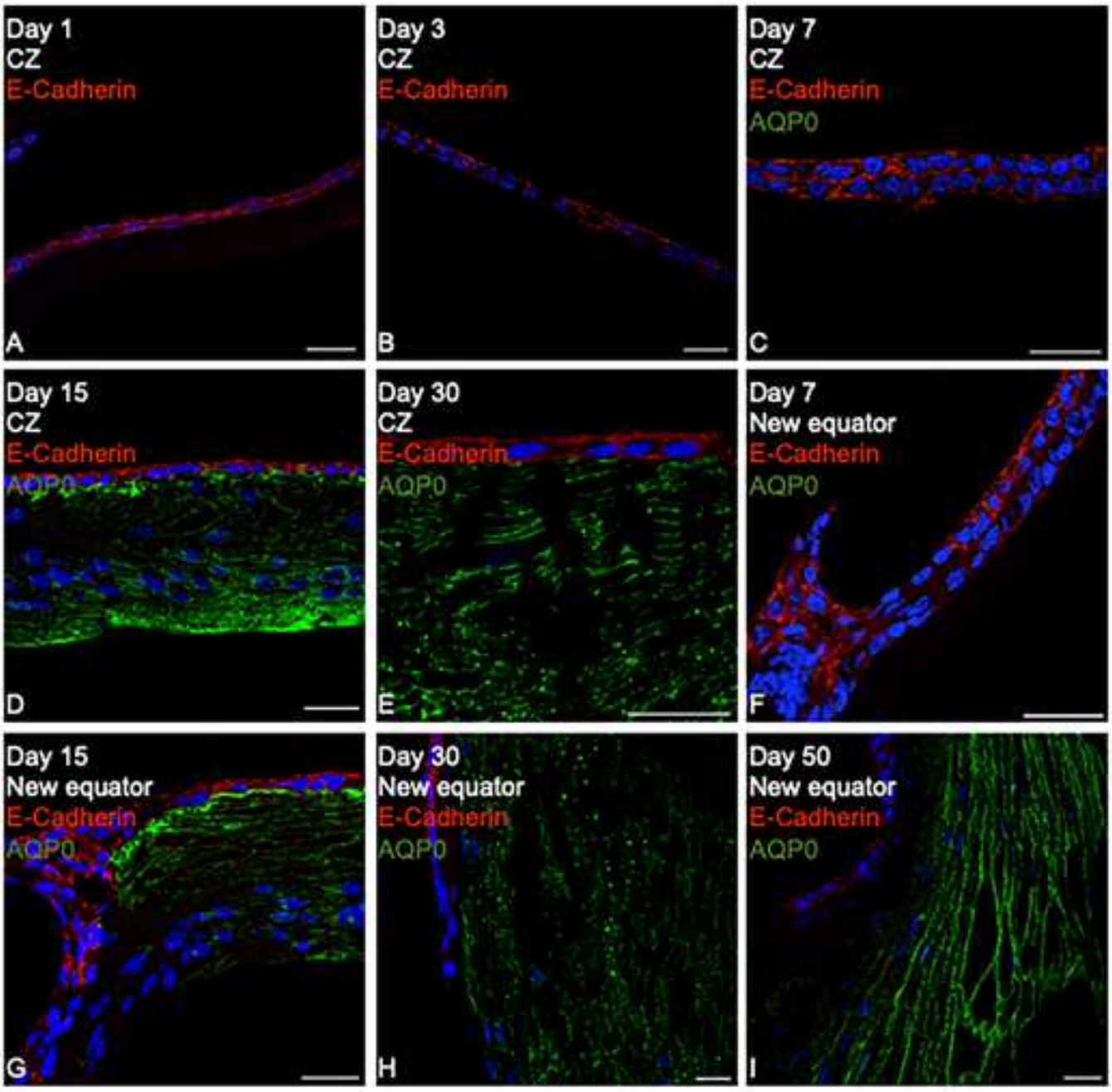

Figure 6. Wu et al

Figure 7

Click here to access/download;Figure;Figure7_WuEER21_600dpi.tif

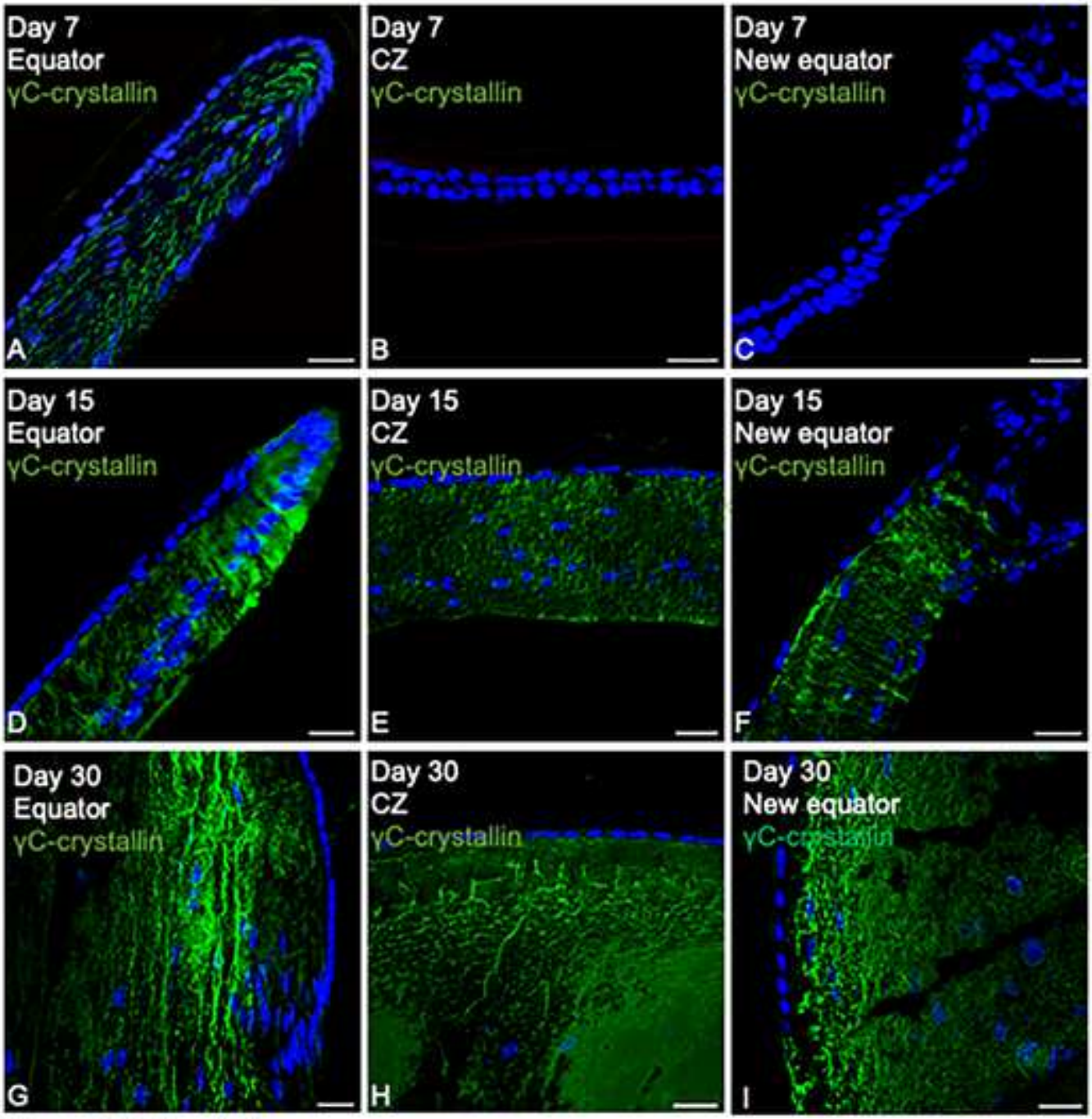

Figure 7. Wu et al

Figure 8

Click here to access/download;Figure;Figure8_WuEER21_600dpi.tif

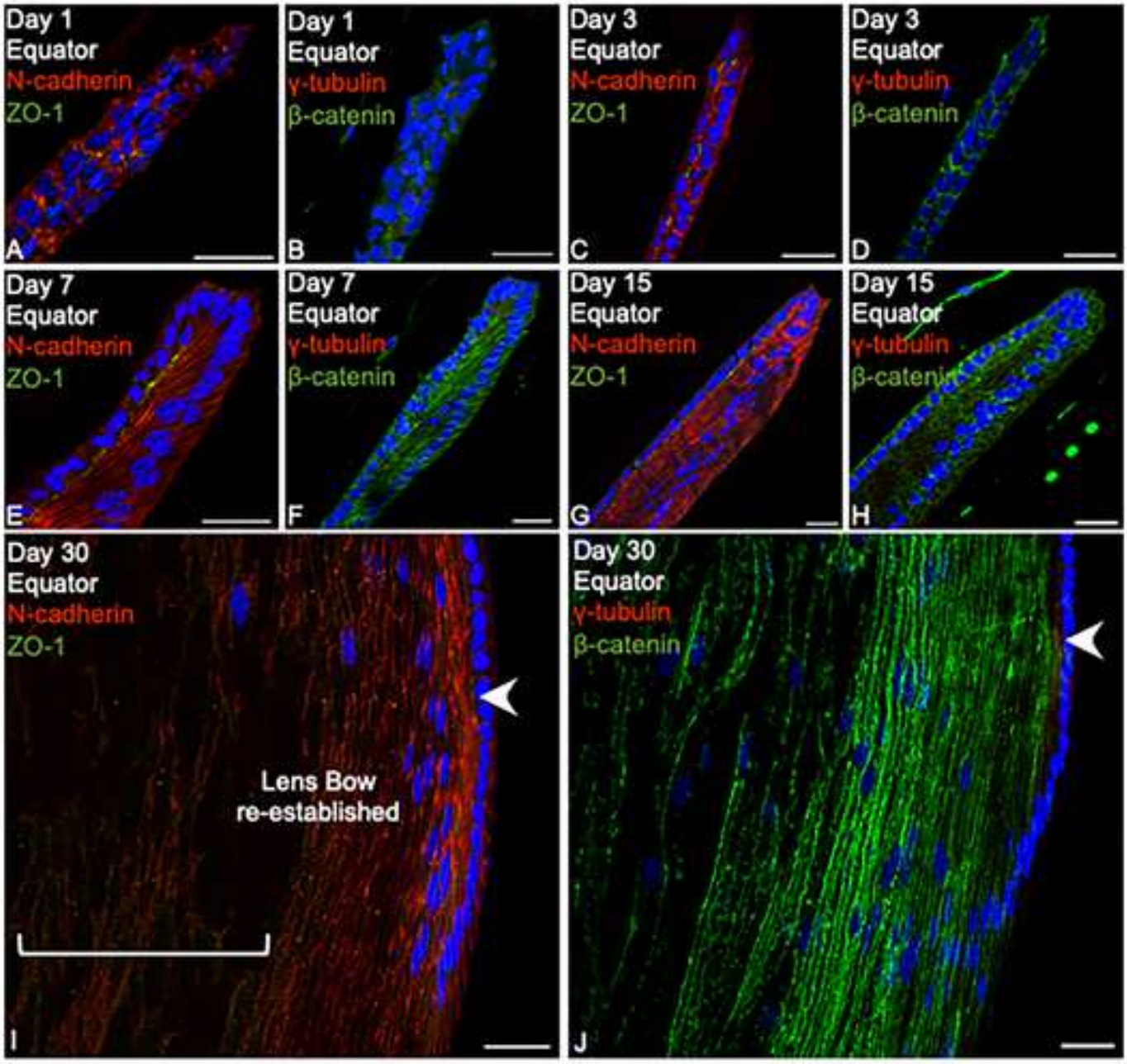

Figure 8. Wu et al

Figure 9

Click here to access/download;Figure;Figure9_WuEER21_600dpi.tif

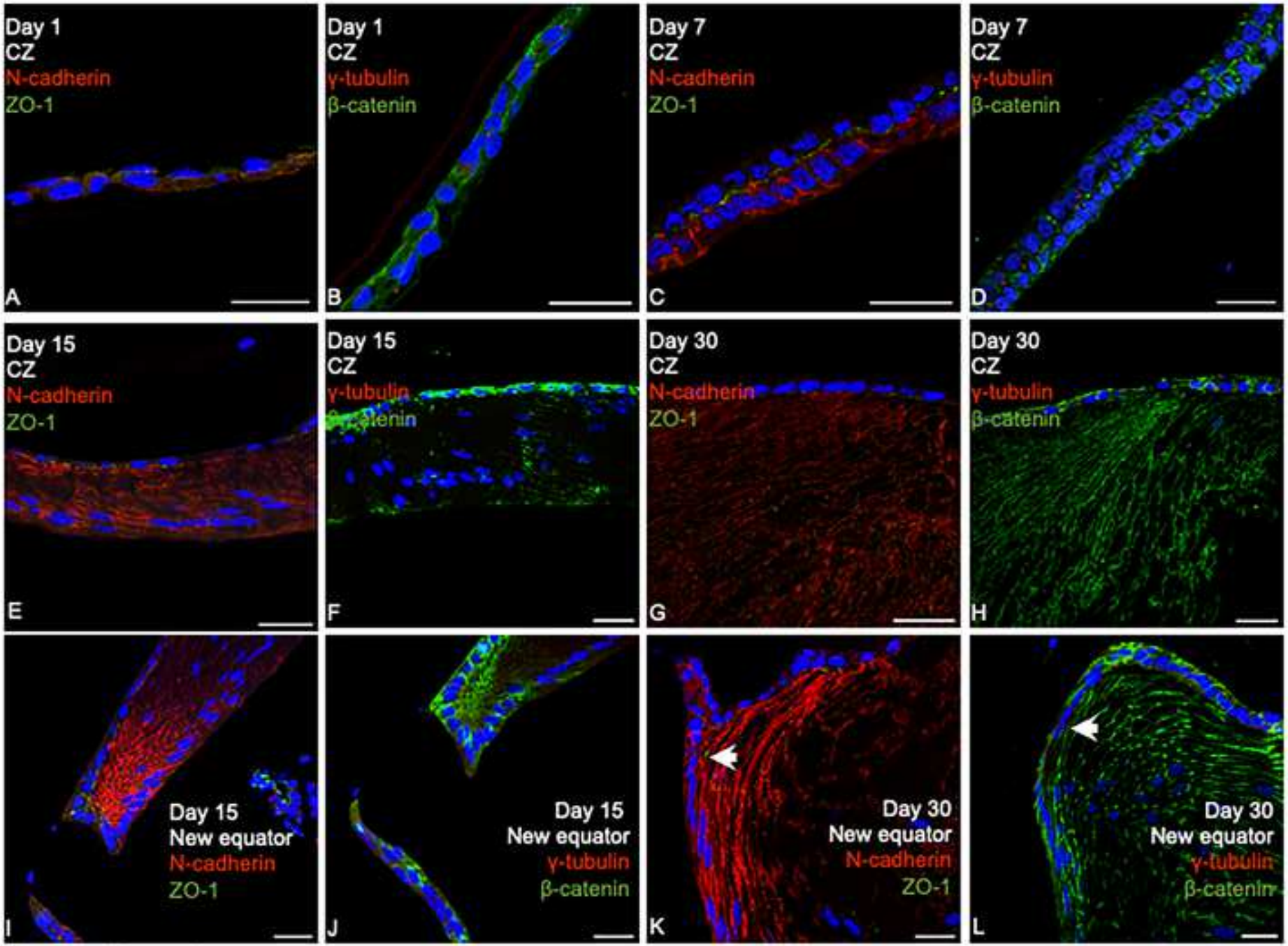

Figure 9. Wu et al

Figure 10A-G

Click here to access/download;Figure;Figure10A-G_WuEER21_600dpi.tif

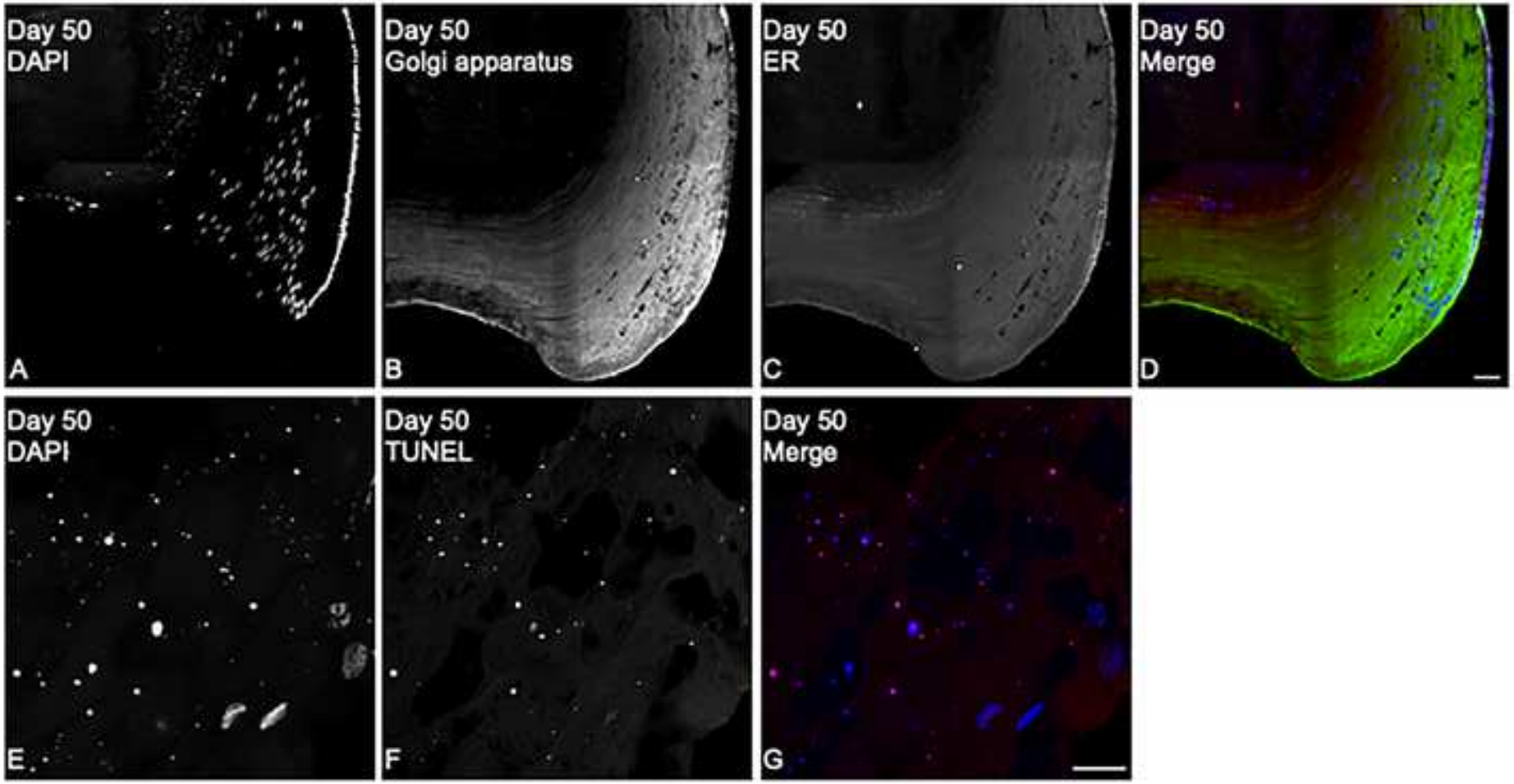

Figure 10. Wu et al

Figure 10H. Lens Regeneration in the Rat

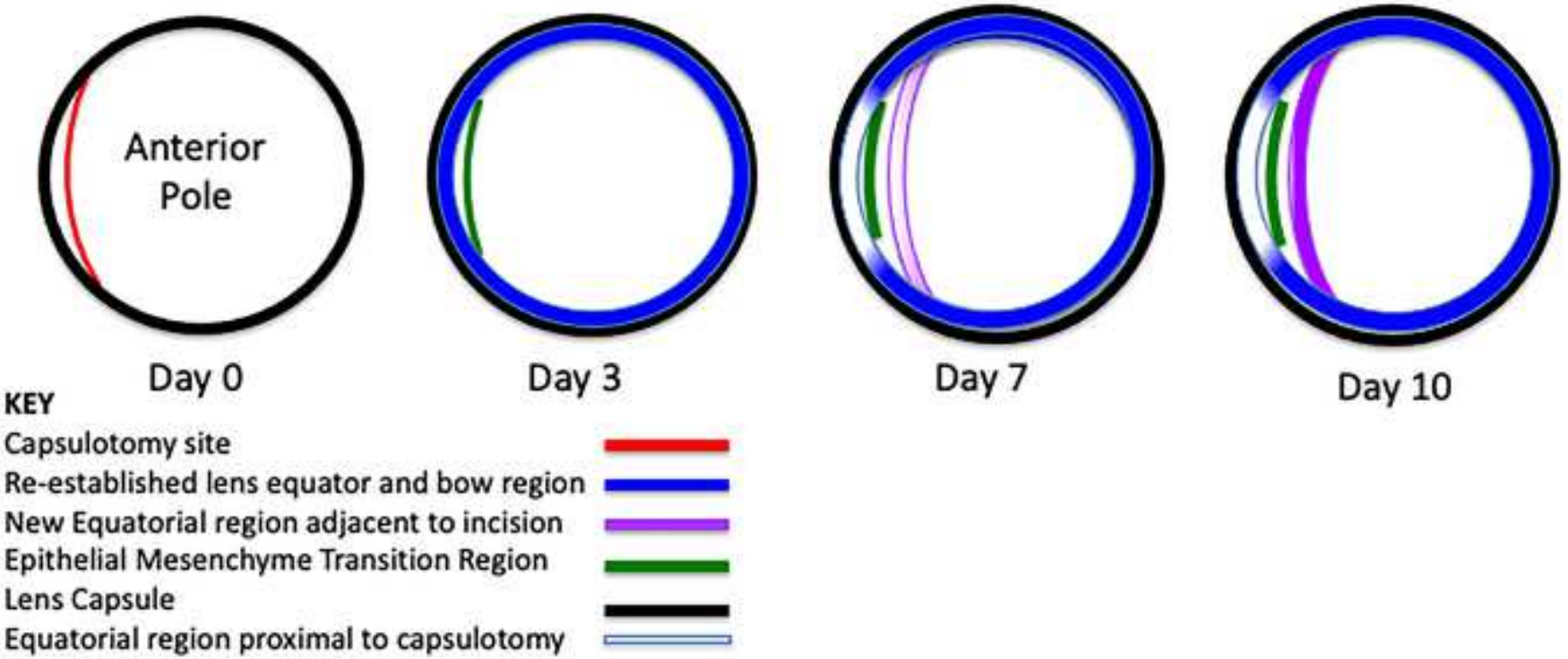

Outside-In Progression of fiber cell elongation

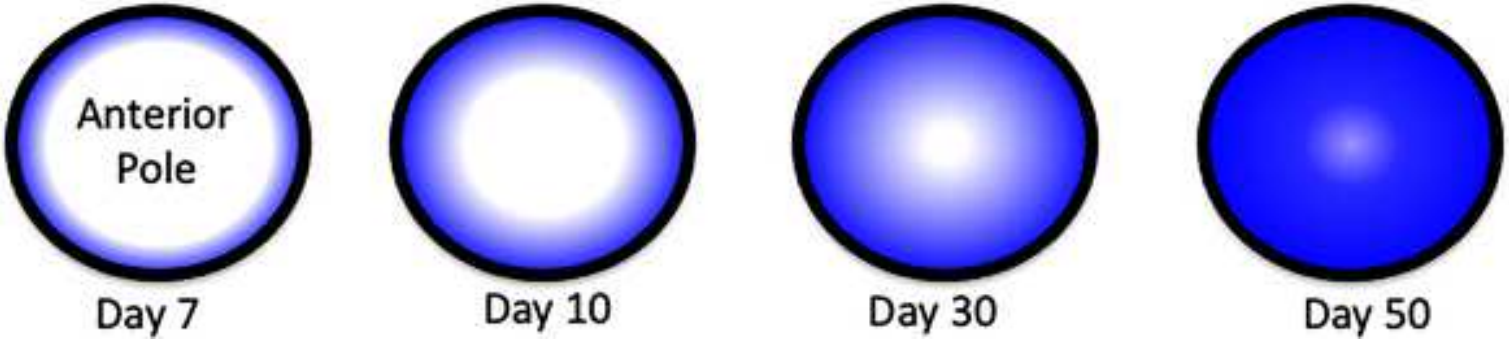

Figure 11

Click here to access/download;Figure;Figure11_WuEER21_600dpi.tif

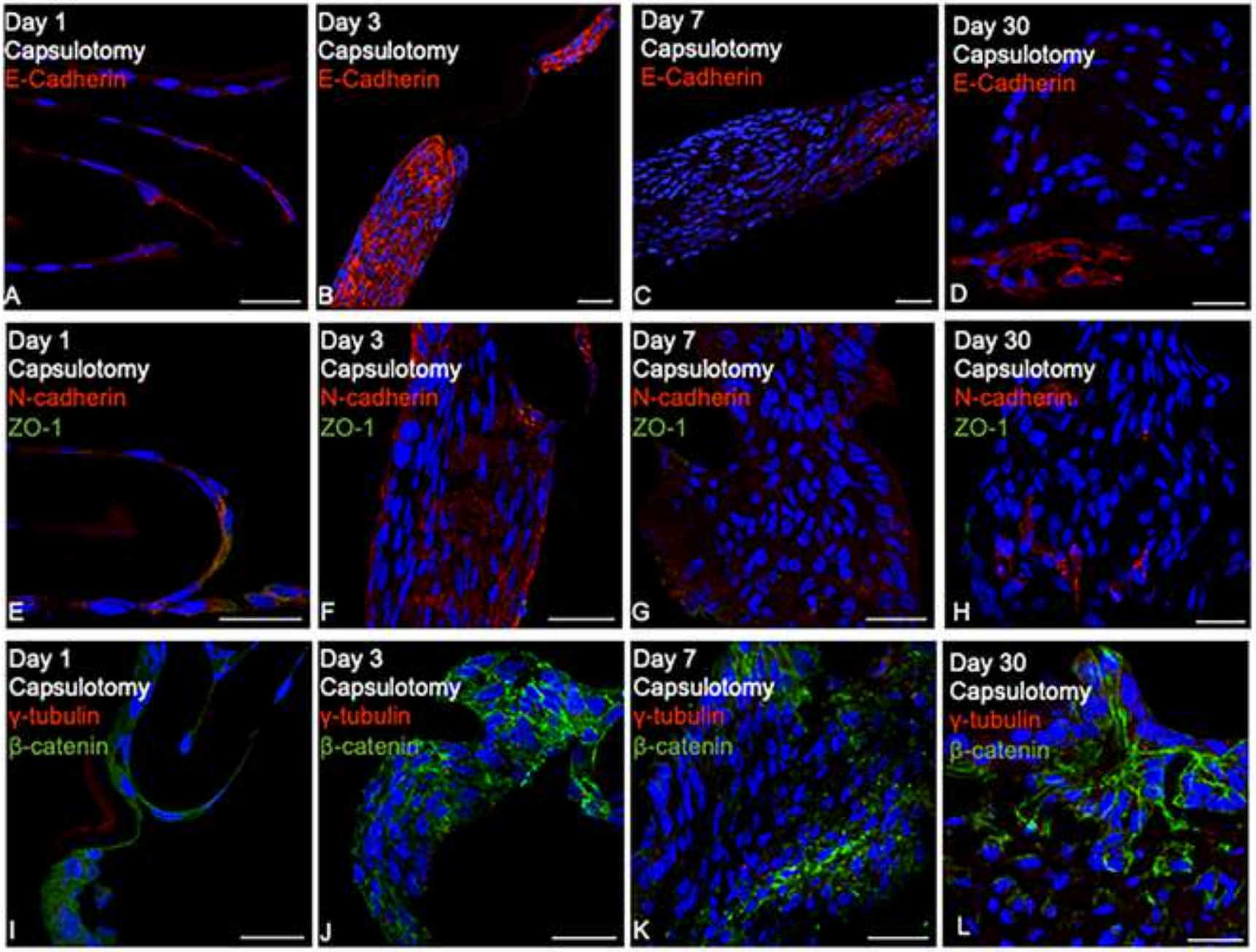

Figure 11. Wu et al

Figure 12

Click here to access/download;Figure;Figure12_WuEER21_600dpi.tif

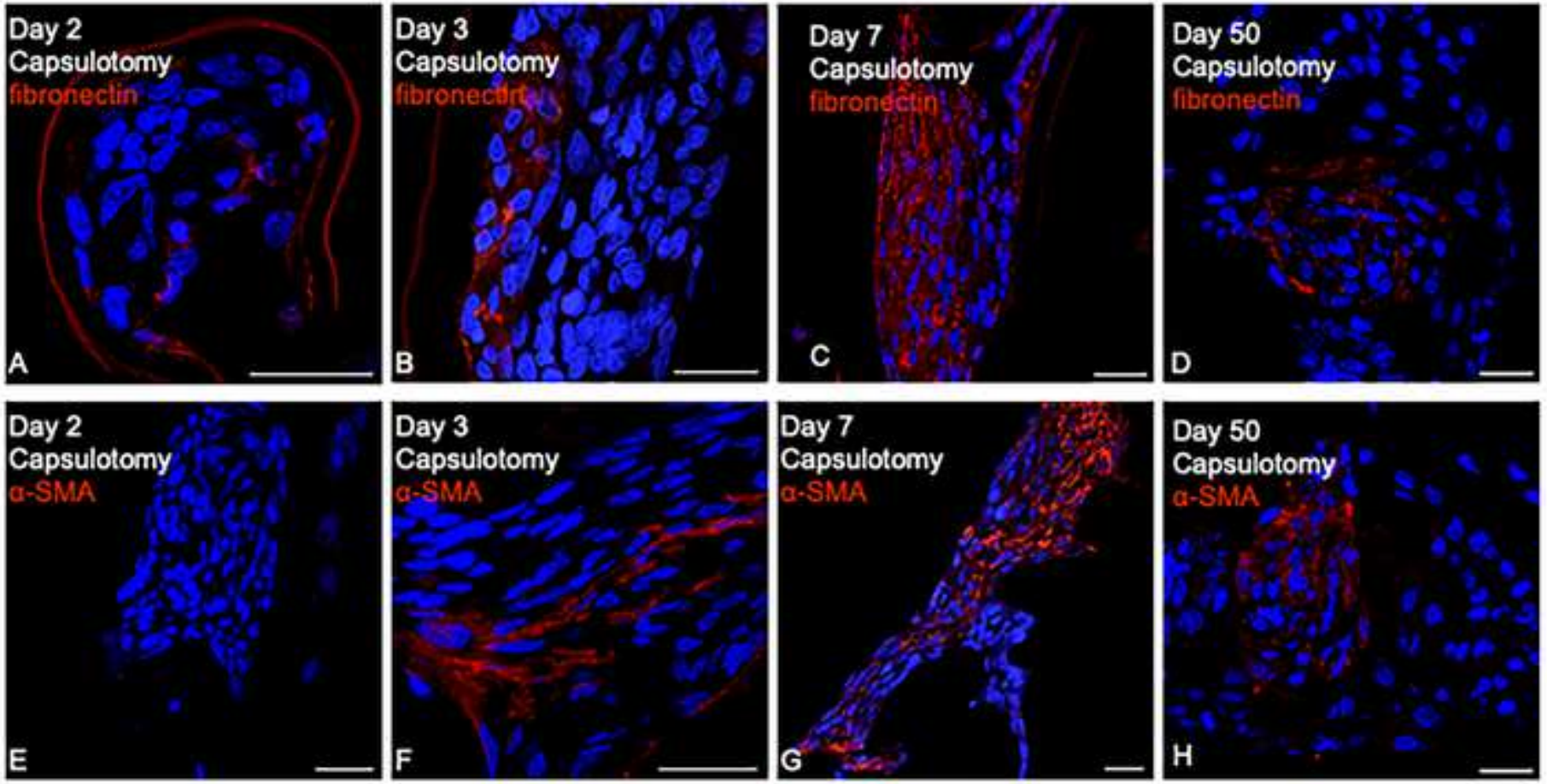

Figure 12. Wu et al

Supplementary Figure 1

Supplementary Figure 2

The importance of the Epithelial Fibre Cell Interface to lens regeneration in an *in vivo* rat model and in a human bag-in-the-lens (BiL) sample.

Weiju Wu[a], Noemi Lois[b], Alan R. Prescott[c], Adrian P. Brown[a], Veerle Van Gerwen[d], Marie-José Tassignon[d, e], Shane A. Richards[f], Christopher Saunter[g], Miguel Jarrin[a], Roy A. Quinlan[a]

[a] Department of Biosciences, South Road, Durham University, Durham DH1 3LE, England, UK

[b] Wellcome-Wolfson Institute for Experimental Medicine, Queens University Belfast, 97 Lisburn Rd, Belfast BT9 7BL, Northern Ireland, UK.

[c] Dundee Imaging Facility & Division of Cell Signalling and Immunology, School of Life Sciences, University of Dundee, Dundee DD1 5EH, Scotland, UK.

[d] Faculty of Medicine and Health Sciences, University of Antwerp, Antwerp, Belgium.

[e] Department of Ophthalmology, Antwerp University Hospital, Edegem, Belgium.

[f] School of Natural Sciences, University of Tasmania Hobart TAS, Australia.

[g] Department of Physics, Durham University, Durham DH1 3LE, England, UK.

Corresponding author:

Roy A. Quinlan, Department of Biosciences, Durham University, South Road, Durham DH1 3LE, United Kingdom.

Email: r.a.quinlan@durham.ac.uk

Noemi Lois, Queens University Belfast, University Road, Belfast BT7 1NN, Northern Ireland, United Kingdom.

Email: noemilois@qub.ac.uk

ABSTRACT

Human lens regeneration and the Bag-in-the-Lens (BIL) surgical treatment for cataract both depend upon lens capsule closure for their success. Our studies suggest that the first three days after surgery are critical to their long-term outcomes. Using a rat model of lens regeneration, we evidenced lens epithelial cell (LEC) proliferation increased some 50 fold in the first day before rapidly declining to rates observed in the germinative zone of the contra-lateral, un-operated lens. Cell multi-layering at the lens equator occurred on days 1 and 2, but then reorganised into two discrete layers by day 3. E- and N-cadherin expression preceded cell polarity being re-established during the first week. Aquaporin 0 (AQP0) was first detected in the elongated cells at the lens equator at day 7. Cells at the capsulotomy site, however, behaved very differently expressing the epithelial mesenchymal transition (EMT) markers fibronectin and alpha-smooth muscle actin (SMA) from day 3 onwards. The physical interaction between the apical surfaces of the anterior and posterior LECs from day 3 after surgery preceded cell elongation. In the human BIL sample fibre cell formation was confirmed by both histological and proteome analyses, but the cellular response is less ordered and variable culminating in Soemmerring's ring (SR) formation and sometimes Elschnig's pearls. This we evidence for lenses from a single patient. No bow region or recognisable epithelial-fibre cell interface (EFI) was evident and consequently the fibre cells were disorganised. We conclude that lens cells require spatial and cellular cues to initiate, sustain and produce an optically functional tissue in addition to capsule integrity and the EFI.

Key words: lens regeneration, cataract surgery, bag in the lens, cadherin, tubulin, AQP0, epithelial mesenchymal transition, posterior capsule opacification.

INTRODUCTION

Regeneration replaces lost or damaged tissue. In the case of the eye lens, regeneration can result in the formation of a transparent or partly transparent lens with similar morphology and cell structure to the structure it replenishes. For LECs to be regeneration-competent (Gwon, 2006; Liu et al., 2020b; Vergara et al., 2018), the integrity of the lens capsule is thought to be critical (Lin et al., 2016; Lois et al., 2010; Tan et al., 2017). Apposing anterior and posterior capsule surfaces encourage the regeneration-like response of LECs (Lois et al., 2010; Tan et al., 2017; Wormstone et al., 2020). When optimised, lens regeneration following fibre cell extraction can generate an optically functional lens (Liu et al., 2020b; Lois et al., 2010; Ruan et al., 2020). This has been observed in a very wide range of animals (Henry and Hamilton, 2018; Lois et al., 2010; Vergara et al., 2018), including humans (Lin et al., 2016; Liu et al., 2020b). Under these circumstances no intraocular lens (IOL) is implanted and no additional tension is placed upon the lens capsule (Berggren et al., 2021; Burd et al., 2017) or zonules (Chen et al., 2019). In such cases, the regenerative response leads to the formation of an optically functional tissue (Liu et al., 2020b; Lois et al., 2010; Ruan et al., 2020). Nevertheless around the incision site in the lens capsule, there is a wound healing rather than a regenerative response (Liu et al., 2020b; Lois et al., 2010), suggesting that the local environment determines the lens epithelial cells (LECs) response. Here we have compared a lens regeneration model in the rat with the Bag in the Lens (BIL) approach. Both generate capsule delimited, closed environments where regenerative responses occur (Lois et al., 2010; Tassignon et al., 2002).

Cataract surgery involves the implantation of an intraocular lens (IOL), but requires an anterior curvilinear capsulorrhexis (i.e. removal of the centre of the anterior lens capsule, irreversibly). This permanently compromises the resulting lens compartment and forces a robust wound healing response that then leads to a complication called posterior capsule opacification (PCO; (Wormstone et al., 2020)). In both animal models (Alon et al., 2014; Lois et al., 2003; Saika et al., 2001) and patients (Wormstone et al., 2020), a partial regenerative response is also seen as evidenced by Soemmerring's Ring formation (SR; (Kappelhof et al., 1985)). This is usually not the most disruptive aspect of PCO (van Bree et al., 2011; Wormstone et al., 2020) as it is usually behind the pupil at the lens periphery. The SR contains fibre cells as well as some degenerating cells (Kappelhof et al., 1985). As cataract surgery does not intend for lens regeneration to occur, the LECs response is different when the lens capsule is sealed or the capsulotomy minimised (Lin et al., 2016; Lois et al., 2010; Tan et al., 2017).

The BIL approach is designed to generate a sealed lens capsule compartment (Tassignon et al., 2002), which would then be expected to encourage the regenerative response by LECs (Lin et al., 2016; Tan et al., 2017). As the surgery involves creating curvilinear rhexes in the anterior and posterior lens capsule followed by the implantation of an IOL that seals both capsule edges, the regenerative response is then confined to this delimited space (Van Looveren et al., 2015) which we term the BIL periphery. Fibre cells are formed (Tassignon et al., 2002; Werner et al., 2010), but they are nevertheless disorganised just like the SR that can be formed following conventional "lens in the bag" (LIB) IOL implantation (Kappelhof et al., 1985; Werner et al., 2010). Why the BIL surgery

resulted in SR formation rather than a lens-like structure (Tassignon et al., 2002; Werner et al., 2010) has yet to be determined.

These data suggest that factors in addition to capsule integrity are important to lens regeneration (Kumar et al., 2019; Lois et al., 2010; Petrova et al., 2020; Vaghefi and Donaldson, 2018). Thus far details of the cell-cell interactions that accompany lens regeneration and how these differ to the wound healing response seen at the capsulotomy site have not been reported (Huang and Xie, 2010; Lin et al., 2016; Tan et al., 2017). We have compared fibre cell formation in a BIL sample to a lens regeneration model in rats. Proteomic analysis of an archived, formalin-fixed, BIL sample from a single patient confirmed a lenticular expression pattern. Histological analyses of the BIL sample also confirmed that fibre cells are disorganized throughout the lens periphery, variable both in width and electron density and thus quite different to a normal, unoperated lens (Freel et al., 2003; Taylor et al., 1996). A recognizable bow region was not observed and neither was an epithelial cell-fibre cell interface. These are prominent features in the lens regeneration model, due to the re-establishment of LEC polarity a week after surgery as seen by cadherin expression patterns. Fibre cell formation started with LECs located on the posterior lens capsule adjacent to the equator and proceeded inwards to the lens centre. LECs at the capsulotomy site proliferated fast, forming multilayers and expressing α-SMA and fibronectin, but E-/N-cadherin expression decreased and all but disappeared. These data show capsule integrity is important to the observed LEC responses, but so too is the apical apposition of LECs to regenerate a bow region and epithelial-fibre cell interface (EFI). Lastly, though fibre cell formation is observed in BIL samples, capsule integrity alone is clearly insufficient. The EFI, 3D organisation and long-term viability of

the regenerated fibre cells were adversely affected. Collectively these data suggest that capsule integrity is only part of the local environment needed to support lens regeneration.

MATERIALS AND METHODS

Bag in the Lens (BIL) samples

This study received ethics committee approval from the Antwerp University and informed consent received from the patients. The use of human tissue in this study was in accordance with the guidelines prescribed by the Declaration of Helsinki. The surgical procedures were performed as previously described (Tassignon et al., 2002; Werner et al., 2010) and reviewed recently (Tassignon et al., 2019). The important points are that the centre of the anterior and posterior lens capsules are removed, with the IOL sealing the exposed edges together in much the same way as a wheel rim seals the tyre (Figure 1A). A follow-up slit lamp image from the eye of one patient after 6 months (patient A, female age 65.5 years) following surgery is presented. The archival samples used for proteomic and histological analyses came from a male patient diagnosed with Korsakoff syndrome (age 76 at time of death) who died in 2016, 4.5 years following BIL implantation, representing the longest post-operative time for the histological and proteomic analysis of a BIL sample (Werner et al., 2008; Werner et al., 2010). The eye was enucleated, immersed in 4% (w/v) neutral buffered (pH6.9) formaldehyde solution. A Miyake-Apple posterior view of the lens (Apple et al., 1990) was recorded before proteomic and histological analyses. The sample was stored at 4 ^{0}C in this solution until required four years later for the studies presented here.

Proteomic analysis of BIL sample

Sample digestion to generate peptides from 4 different locations around the capsular periphery of the BIL was as described (Coscia et al., 2020), with the following

modifications. A Covaris M220 instrument using Adaptive Focused Acoustics was used to disrupt the formaldehyde fixed lens tissue in a microTUBE AFA Fiber Pre-Slit Snap-Cap (130 µL). Lens material was snap frozen, crushed and then added to 130µl of 50% (v/v) TFE, 0.3 M Tris-HCl pH 8.0 and 5 mM EDTA. It was sonicated in 2 bursts of 100cycles at 75W (peak incident power) and a 10% duty factor for 6 min at 20 ^{0}C. Samples were then heated (90°C, 90min) in a ThermoMixer (Eppendorf) before being sonicated a second time. Protein extracts were then reduced with 5 mM 1,4-dithiothreitol (DTT) for 20 min before alkylation with 25 mM 2-iodoacetamide (IAA) for another 20 min (1,500 rpm).

Samples were assessed for the efficiency of protein extraction from the formaldehyde fixed material by SDS PAGE on 4-12% (w/v) NuPAGE Bis-Tris gels (ThermoFischer Scientific). Bands were excised for subsequent proteomic analysis by LC-MS (Supplementary Figure 1) and confirmed the presence of αA-, αB-, βA4, βB2- and γS-crystallins in these BIL extracts.

Trypsin was added at a 1:50 ratio to an aliquot of the sample. Protein digestion was performed overnight at 37°C. On the following day, digestion was stopped by adding trifluoroacetic acid (TFA). The final clean-up StageTips contained two SCX filter pieces in place of SDB-RPS (Rappsilber et al., 2007). LC-MS analysis of peptides was performed on a SCIEX TripleTOF 6600 mass spectrometer linked to an Eksigent nanoLC 425 chromatography system via a 50-micron ESI electrode in a DuoSpray source (SCIEX). Sample injection and peptide separation used a trap and elute method flowing at 5 µl/min. Peptides were loaded and washed on a YMC TriArt C18 guard column (1/32", 5 µm, 5 × 0.5 mm) and online chromatographic separation performed over 33 min on a YMC TriArt

C18 column (1/32", 12 nm, S-3 µm,150 × 0.3 mm). The gradient profile was as follows: a linear gradient of 5–35% (v/v) acetonitrile, 0.1% (v/v) formic acid over 20 min, shift to 80% (v/v) acetonitrile, 0.1% (v/v) formic acid over 2 min, a column wash for 3 min before returning to 5% (v/v) acetonitrile, 0.1% (v/v) formic acid over to 2 min and re-equilibration for 6 min. Data-dependent LC-MS-MS acquisition was scheduled between 0.1 and 24 min during this gradient and the source voltage was switched from 5500 to 0 V outside of this period. Each MS cycle consisted of a 250 msec precursor-ion scan from 350 to 1,500 *m*/*z* followed by fragmentation of up to 10 selected ions for 100 msec each to generate MS/MS spectra of 100 to 1,500 *m*/*z* (cycle time 1.3 sec). Switch criteria applied were +2 to +5 ions, of intensity >400 cps, with a rolling exclusion time of 12 sec.

LC-MS/MS peak lists in (.mgf) format were generated from (.wiff) format data files using MSConvert in the ProteoWizard suite of proteomic software tools and peptide/protein identification used PEAKS X+ software (Bioinformatics Solutions Inc). Default precursor and product ion tolerances for a TripleTOF spectrometer were specified, along with the following modifications: fixed - carbamidomethyl [C], variable - oxidation [M], acetylation [N-term], deamidation [NQ], oxidation [HW]. Search databases were a UniProt mouse reference proteome (March 2019, 22,285 entries) plus 194 known proteomic experiment contaminants, or a human reference proteome (February 2017, 20,106 entries) plus 161 contaminants. Peptide FDR was set at 1% and a filter of 2 unique peptides applied to identified proteins.

Histological Analysis of BIL samples

The lens samples that had been formalin-fixed for 4 years were cut into pieces < 1mm^3 and re-fixed in 4% (w/v) paraformaldehyde, 2.5% (v/v) glutaraldehyde in 0.1M sodium

cacodylate buffer (pH 7.2) for 60 min. The pieces were then post-fixed in 1% (v/v) osmium tetroxide in cacodylate buffer for 60 min. En-bloc contrasting was then carried out sequentially with 1% (w/v) tannic acid in cacodylate buffer and 1% uranyl acetate in acetate buffer (pH 6) each for 60 min. Samples were dehydrated through alcohol series, propylene oxide and embedded in Durcupan resin (Fluka). Polymerised resin blocks (48hrs at 60^0C) were sectioned on a Leica UCT ultramicrotome. 500nm thick sections were collected for light microscopy and stained with toluidine blue and subsequent ultra-thin sections (70-80nm) were collected onto pioloform coated copper EM grids. EM sections were contrasted with uranyl acetate and lead citrate and imaged on a JEOL 1200EX transmission electron microscope, digital images were collected on a SIS Megaview III camera.

Animal studies and permissions

For this study, 60 Sprague-Dawley male rats, 200-300 grams, were used, a minimum of 6 per time point in the study. Animal procedures were performed in accordance with Home Office (UK) regulations and conformed the Association for Research in Vision and Ophthalmology (ARVO) Statement for the Use of Animals in Ophthalmic and Vision Research. Surgical procedures were performed only in the right eye of each animal, the contralateral eye serving as a control.

Surgical procedure

The surgery has been previously described in detailed (Lois et al., 2010). In brief, in all operated eyes, a peripheral cambered incision was made in the cornea followed by the injection of 1% (w/v) sodium hyaluronate (Pharmacia and Upjohn, Ltd., UK) into the

anterior chamber. A “smile-shaped” anterior capsulotomy was performed, as peripheral in the anterior lens capsule as possible and then the lens fibre mass was removed. Sodium hyaluronate was then injected into the anterior chamber and over the top of the anterior capsule to achieve apposition between the two lips of the capsulotomy and, thus, closure of the capsular bag. The corneal incision was closed with interrupted 11-0 non-absorbable monofilament suture (Mersilene; Johnson & Johnson Medical Ltd, USA).

EdU labelling

EdU (5-ethynyl-2’-deoxyuridine, 75 mg/kg; #CLK-N001, Jena Bioscience, Germany) was injected intraperitoneally 7 hours prior to the animal’s sacrifice on 0, 1, 2, 3, 7, 10, 15 (6 rats in each group), 30 (9 rats) and 50 (9 rats) days following surgery. The unoperated control lenses were isolated to prepare the lens epithelium flat-mounts according to previous report (Ong et al., 2003). For the isolation of regenerated lenses, zonules were bluntly broken with Vannas scissors in a small area and sodium hyaluronate was injected under the lens to inflate it and to maintain it intact during the amputation of rest zonules. As regeneration was very advanced by day 30 and 50 following surgery, the lens capsule and epithelium from five samples per time point were removed for EdU labelling. The lens mass from these dissected lenses was used for cryosectioning and immunofluorescence microscopy. All the control lens epithelium flat-mounts and regenerated lens samples were fixed in 4% (w/v) paraformaldehyde (PFA). The total nuclei and EdU incorporated nuclei were detected with DAPI (4,6-diamidino-2-phenylindole; Molecular Probe Inc., Eugene, Oregon, USA) and AlexaFluor 488-azide using a Click-iT Kit according to manufacturer’s instructions (Invitrogen). Three to four small incisions were made at the very periphery of the regenerated lens immediately prior to staining to facilitate reagent

penetration into the sample. EdU labelling was then evaluated using a Leica SP5 confocal scanning laser microscope (Leica microsystems, Germany).

Immunofluorescence microscopy

The PFA-fixed samples were cryo-protected in 30% (w/v) sucrose, embedded in OCT and sectioned perpendicularly through the capsulotomy site and equatorial region at 10-12 μm. The sections were permeabilised and incubated with blocking solution (Phosphate Buffered Salts containing 0.1% (v/v) goat serum, 1% (w/v) bovine serum albumin, and 0.1% (v/v) Triton X-100) for 1 hour at room temperature, followed by an overnight incubation with the primary antibodies at 4^0C and 1 hour with the secondary antibodies at room temperature. Images were obtained using a Leica SP5 confocal scanning laser microscope (Leica microsystems, Germany).

The antibodies used in the present study were obtained from the following sources: mouse anti-E-cadherin and anti-N-cadherin monoclonal antibodies (BD Transduction Laboratories Cat #610181 and 610920 respectively); rabbit anti-β-catenin polyclonal antibody (Sigma-Aldrich Cat #C2206); mouse anti-γ-tubulin monoclonal antibody (GTU-88; Abcam Cat #ab11316) and rabbit anti-fibronectin polyclonal antibody (Abcam Cat #ab2413); rabbit anti-aquaporin 0 (AQP0) polyclonal antibody (Alpha Diagnostic, San Antonio, TX); rabbit anti-ZO-1 polyclonal antibody (Invitrogen Cat #40-2200); rabbit anti-Golgi apparatus polyclonal antibody (a kind gift from Dr. Rumaisa Bashir; Abcam rabbit anti-TGN-46 Cat #ab16059); mouse anti-ER monoclonal antibody (gift from Dr. Adam Benham; PDI mouse mAb RL90; Cat #ab2792,); mouse anti-α-smooth muscle actin (α-

SMA) monoclonal antibody (Invitrogen Cat #14-9760-82); rabbit polyclonal anti-γC-crystallin has been described previously (Pigaga and Quinlan, 2006); primary antibody detection was achieved using goat anti-mouse TRITC, goat anti-mouse FITC and goat anti-rabbit TRITC (all from Sigma-Aldrich); goat anti-rabbit FITC (Wilkson); anti-mouse CY5 (Jackson Immunoresearch Laboratories).

TUNEL assay

The regenerated lenses on day 30 and 50 were sectioned and fixed in PFA for 20 minutes. They were then permeabilised with 0.1% (v/v) Triton X-100 for 2 minutes on ice. TUNEL staining was carried out by using an *in situ* cell-death detection kit, TMR red, according to manufacturer's instructions (Roche Diagnostics GmbH, Germany).

Statistical analyses

In order to analyse the proliferation index in the regenerated lenses, four images per lens from the equator, central zone (CZ) and the capsulotomy site were randomly obtained. In the control lens epithelium flat-mounts, images were taken from the CZ and equator. The EdU-positive cells and total cell number in each image were counted by ImageJ and delineator, a software specially developed by our group to count LECs. The proliferation index in each region was obtained by dividing the EdU-positive cell number by the total cell number. We defined *p(t)* to be the proportion of cells labelled EdU positive at time *t* days after surgery. For a given region of the eye (e.g., equator or central zone). we assumed this time-series had the form:

$$logit\ p\ =\ ln\left(\frac{p}{1-p}\right) = \beta_0 + \beta_1 t + z\beta_2 exp(-\alpha t).$$

Here, *z* is a binary value that indicates if the eye is the control (z=0) or had surgery (z=1). For the control eye, the change in the proportion of EdU positive cells is consistent with the logistic function. Surgery adds EdU positive cells (quantified by β_2), which decay to baseline levels at rate α. This equation is modified to account for overdispersion with respect to the binomial distribution by adding an observation level random effect to the right side. Similarly, a rat-level random effect is added to account for repeated measures on rats, and a time by region random factor is also added to account for the high variation in the indices observed between days and regions. We assumed that EdU frequency at the capsulotomy site eventually decayed to a baseline level associated with the equator. This model has 13 parameters, which were estimated using Bayesian methods, based on Monte Carlo sampling. We used R (R Core Team, 2020) and rstan (Stan Development Team, 2020) to perform the statistical analyses. We specified relatively uninformative priors for all parameters so that the posterior distributions were strongly dependent on the data. Posterior parameter distributions were based on 1000 samples after a 1000 sample burn-in (see Supplementary Material).

RESULTS

Proteomic and histological characterisation of the Bag in the Lens (BIL)

The BIL approach implants an IOL to seal the edges of the two capsulorrhexis made in the centre of the anterior and posterior lens capsules and therefore effectively acting like the rim in a wheel. After anterior and posterior rhexes have been removed, the lens capsule is akin to the tyre, sealed in place by the wheel rim, the IOL. The aim is to create a closed compartment to physically confine the lens cells that are retained after cataract surgery to the lens periphery and delimited by the residual anterior and posterior lens capsules (Figure 1A). As can be seen from images of one patient's eye after 6 months (Figure 1B) this results in the formation of a relatively transparent lens perimeter around the implanted IOL due to the formation of the SR (Tassignon et al., 2002). Some Eschnig's Pearls can be seen (Figure 1B, arrow), and within the SR there is evidence of localised loss of transparency in the SR, primarily at the most distal edge of the lens rim (Figure 1B arrowheads).

Opportunities to analyse the biochemical and cell biological changes that accompany SR formation in the lens perimeter after BIL surgery are uncommon (Tassignon et al., 2019; Werner et al., 2008; Werner et al., 2010), much more so than post-surgery clinical assessments where a full age range can be assessed (Tassignon et al., 2011; Van Looveren et al., 2015). A BIL implant in a 15 year old is shown (Figure 1B). By comparing with results presented elsewhere (Tassignon et al., 2019) there are similar clinical outcomes across the age range. We had access to one sample from an 85 year old (Figure 1D), from which we present an initial proteome (Table 1) and histological analysis (Figure 2). This sample is the longest postoperative time for a BIL sample to be analysed

in this way. Our histological data confirm, but add to, the observations made on four other samples with shorter post-operative times (Werner, 2019; Werner et al., 2008; Werner et al., 2010).

By creating a contained environment, SR formation is both encouraged as well as confined so that lens cells do not encroach upon the implanted IOL. Toluidine blue staining of the distal region of the lens perimeter revealed a lack of organisation in an area where the lens bow should have been retained but is no longer present (Figure 2A). LECs are found on both the anterior (Figure 2A, a) and posterior (Figure 2A, p) lens capsules and the fibre cells show a lack of organisation, with longitudinal and cross-section profiles evident within this section. Samples of the lens perimeter were processed for electron microscopy (Figure 2B-F) for a more detailed cell biological assessment. The discord in fibre cell differentiation is evident in Figure 2B. Those fibre cells most distal from the implanted BIL IOL show variable width (Figure 2B, brackets) and those cells closest to the IOL in various stages of degeneration (Figure 2B, asterisk). In those regions where fibre cells are evident, there are organelle free and membrane specialisations like ball and socket interdigitations (Figure 2C, arrow), but a lack of contrast consistency between adjacent fibre cells is also apparent (Figure 2C, F). Plasma membranes of adjacent fibre cells are tightly apposed and the inter-cellular spacing regular (Figure 2D). In other regions of the lens perimeter (Figure 2E) cell degeneration is observed, a feature also noted by other BIL studies (Werner, 2019). The epithelial cell layer is disorganised, with elongating epithelial cells seemingly adrift from the lens capsule (Figure 2F, asterisks) while underlying elongating fibre cells are variable in both width and cytoplasmic staining (Figure 2F, bracket). Nuclei are retained in some but not all of the

fibre cells in this image and fibre cells make prominent cell-cell junctions with the ends of other fibre cells suggesting that the epithelial-fibre cell interface (EFI) is altered (Figure 2F, brackets). These observations compel the view that cell differentiation is possible after BIL surgery, but it is uncoordinated and variable due to the loss of a recognisable bow region and also dependent upon the cellular location within the SR.

We took advantage of a recently published method to determine the proteome of formaldehyde fixed archival material (Coscia et al., 2020) to confirm that crystallin, cytoskeleton and extracellular matrix (ECM) markers of lens fibre cell differentiation could be detected as was achieved for previous proteomic analyses of congenital cataracts (Van Looveren et al., 2018; Wu et al., 2017). Four samples from different locations around the lens rim (Figure 1D) were taken. The dataset supported the conclusion that fibre cell formation had occurred as evidenced by the range of lens proteins detected (Table 1A). Acetylation, deamidation and oxidation were detected for the α-, β- and γ-crystallins and some of the major cytoskeletal proteins expressed in this 4.5 year old BIL sample (Table 1B). Most have been reported previously and are consistent with the generalised conclusion that such post-translational modifications (PTMs) are part and parcel of long-lived lens proteins (Hains and Truscott, 2010; Schey et al., 2020). We note that some of the PTMs we found would be expected to compromise protein function (DiMauro et al., 2014; Lampi et al., 2014; Nagaraj et al., 2012; Pande et al., 2015; Ray et al., 2017; Serebryany and King, 2014).

Lens regeneration was initiated at the equatorial region, re-establishing the lens bow and producing predominantly transparent lenses.

SR formation is considered a regenerative response (Wormstone et al., 2020) and we decided to compare this to a lens regeneration rat model (Lois et al., 2003; Lois et al., 2010), where previously others had suggested SR formation preceded reforming a transparent eye lens (Huang and Xie, 2010). The lens body was removed via a capsule incision (capsulotomy) and the regenerative response then followed over a 50 day period. Anterior and posterior capsules contact one another postoperatively even on day 1 (Figure 3A), with the exception of the capsulotomy site, where only the posterior capsule was present because the anterior capsule's tendency to curl and retract eg (Liu et al., 1996; Packard, 2019). Lens regeneration occurred in those areas where both anterior and posterior capsule were present (i.e. inferior to the capsulotomy site). The capsular bag filled evenly with lens cells during the first week post-surgery (Figure 3A-C). As the regeneration process progressed, the periphery of the regenerated lens became noticeably thicker than the central area (Figure 3D) and a "donut or bagel-shaped" transparent ring was formed by postoperative day 30 (Figure 3E), reminiscent in shape of the SR formed after BIL surgery. Similar observations have been made by others (Gwon, 2006; Huang and Xie, 2010; Lois et al., 2003). This continued to thicken with time (Figure 3F; day 50). One of the eight regenerated lenses showed small opacities and "cavities" (Figure 3F), indicating that lens regeneration is not always perfect for animal (Gwon, 2006; Gwon et al., 1999) or human lenses (Liu et al., 2020b), making further surgery necessary (Wu et al., 2017). No nuclear cataracts were observed in any of the regenerated lenses at day 50. An opaque scar with wrinkles radiating from it was observed at the capsulotomy site in all cases from day 2 to day 15 post-operatively (Figure 3B-D). Some transparent lens tissue was seen bulging from the lens adjacent to the

capsulotomy area in the isolated regenerated lenses of day 30 and 50 (Figure E-F), but this was not analysed any further.

Cell proliferation occurred in most lens cells immediately following surgery but became restricted to the lens equator as regeneration progressed.

In flat-mounts of the unoperated, contralateral lens epithelium, cell proliferation was mainly restricted to the lens equator as has been observed previously (Kalligeraki et al., 2020; Wu et al., 2015). At day 1 following surgery, a burst of cell proliferation occurred throughout the entire lens epithelium (Figure 4A). The proliferation indexes at the equator, central zone (CZ) and capsulotomy site were 74.62%, 46.32% and 67.49% respectively compared with 3.37% and 0.62% at the lens equator and CZ respectively of the contralateral control (unoperated) lenses (Figure 4C). This increase in cell proliferation decayed rapidly over the next two days, especially in the equator and CZ (Figure 4B, C) and after 7 days had returned to a baseline level that remained so over the next 3 weeks (Figure 4C). Such data would usually be analysed using a generalised linear model (GLM), but the decay effect we observed cannot be readily described by the linear component of a GLM and so we undertook a Bayesian analysis to build a customised model to accommodate the decay pattern we observed (Figure 4C). The model confirmed that the proliferation rates for the CZ and equatorial regions of the unoperated lens were different to higher rates observed at the lens equator (Figure 4C; Control), in agreement with previous studies (Kalligeraki et al., 2020; Wu et al., 2015). The model confirms that the proliferation index at the equator of the regenerated lenses spiked on day 1 before returning to levels observed in the control equatorial region of unoperated lenses from day 7 onwards (Figure 4C). LECs at the capsulotomy site, which is also close to the

equator, showed a similar trend (Figure 4C). The LECs in the CZ of the regenerated lenses also spiked on the first day, but then decayed more rapidly that those cells at the equator eventually reaching those proliferation rates observed in the CZ of control lenses by day 30 (Figure 4C). These data indicate that the proliferation rate of the LECs in the different regions of the regenerating lens, including the capsulotomy site, each have a characteristic response to the surgical removal of the fibre cells.

Cells reorganised into two layers and fibre cell differentiation and elongation proceeded from the equator to the epicentre of the regenerating lens

In the capsular bag obtained immediately after surgery (day 0), a monolayer of LECs was present underlying the anterior lens capsule and covering the posterior capsule. The most peripherally located cells at the lens equator lost expression of E-cadherin (Figure 5A), a LEC marker and became N-cadherin positive, a fibre cell marker (Data not shown). On day 1 post-surgery, the lens cells at the equator became multi-layered (Figure 5B and Figure 8A, B), which was seen also on day 2 (Figure 5C). By day 3, however, these multilayers had become reorganised into two monolayers of cells, with their apical surfaces apposed to form a new Epithelial-Fibre cell Interface (EFI; Figure 5D and also Figure 8C, D). We observed cells with condensed or fragmented nuclei in areas where multi-layered LECs persisted (Figure 5E, arrowheads). Both E- and N-cadherin were expressed in all the equatorial lens cells during the first three days of the regeneration process (Figures 5 and 8). Over the next 3-4 days, this bi-layered cell organisation was maintained, but by day 7, E-cadherin expression had become restricted to the anterior LECs (Figure 5F) and N-cadherin was enriched in the posterior LECs (Figure 8E). Those cells on the posterior lens capsule have elongated (Figure 8E, F) and had begun to

express the fibre specific markers, aquaporin 0 (AQP0; Figure 5F) and γC-crystallin (Figure 7A). Fibre cell formation occurred at the lens equator and led to the reformation of a bow region as a recognisable feature of the regenerating lens. Fibre cell elongation continued across the CZ on day 15 (Figures 3G, 5D and 6G), explaining the donut/bagel-like appearance after 15 days of regeneration (Figure 3D). A more rounded shape was acquired by day 30. Cells at the equator of these lenses (Figures 3H, 5G and 6E) were similar in morphology and expression characteristics as seen in un-operated lenses. By day 50 the nuclei in the elongating fibre cells in the equatorial region of the lens were observed to form the iconic bow (Figure 5I) as expected for cross sections of animal lenses.

The lens cell organization in the CZ mimicked the observations made for the lens equator. On the first day postoperatively, E-/N-cadherin staining demonstrated that two distinct monolayers of flat LECs start to form here (Figures 6, 7 and 9). E-cadherin was expressed in LECs on both capsule surfaces at the CZ at day 7 (Figure 6C), but only the LECs on the posterior capsule expressed N-cadherin (Figure 9C). Neither AQP0 nor γC-crystallin was present in these N-cadherin positive cells at day 7 (Figures 6C and 7B). By day 15, however, cells on the posterior lens capsule had elongated and the fibre cell differentiation markers AQP0 (Figure 6D) and γC-crystallin (Figure 7E) were expressed. The epithelial cells on the anterior lens capsule retained their monolayer organisation, at these time points and the differentiation markers and DAPI stain for nuclei show that it is those cells located on the posterior lens capsule in the lens that are responsible for expanding tissue thickness in this central region of the regenerating lens. The CZ became thicker by day 30 and day 50 (Figures 3E, 3F, 7H and Figure 10). The LECs on the

anterior lens capsule remained cuboidal in shape, but the apical cell surfaces remained closely apposed throughout this process (Figures 4E, 5H and 7G).

Adjacent to the capsulotomy site, LEC and fibre cell organisation was similar to that seen at the regenerating lens equator (Figure 6F-I). We define this region as the "new equator". Here fibre cell elongation and differentiation were delayed slightly. The expression of AQP0 and γ-crystallin was detected on day 15 (Figures 6G and 7F) rather than on day 7 (Figures 6F and 7C) at equatorial regions distal to the capsulotomy site.

Cell polarity was established and maintained during lens regeneration

On day 1 post-surgery at the lens equator, the polarity marker ZO-1, was no longer clearly located at the apical ends of epithelial cells and fibre cells as would be expected (Sugiyama et al., 2008), but rather was found in occasional foci on the membrane interface between neighbouring cells (Figure 8A). Another polarity marker, γ-tubulin, was also altered and was found to have adopted a peri-nuclear location (Figure 8B). Normally this centrosomal marker locates to the apical ends of lens cells in this equatorial region (Dahm et al., 2007). These data suggest that cell polarity has become lost. By day 3, ZO-1 was restricted to the presumptive EFI between the two LEC layers (Figure 8C) with γ-tubulin once more located subapically (Figure 8D). The apical plasma membranes of the anterior LECs tightly apposed those from the corresponding apical surfaces of the posterior LECs as there was no obvious inter-cellular space that would permit hydro-dissection as utilised in lens cataract surgery. The basal ends of the respective LEC layers remained attached to the anterior and posterior capsules. The apical-basal cell polarity was maintained as fibre cell differentiation and elongation proceeded as seen by the day

7 (Figure 8E, F) and day 15 (Figure 8G, H) samples. A typical bow region was reformed at the lens equator by day 30. Both ZO-1 and γ-tubulin signals disappeared from the last 10-12 elongating fibre cells at the equator (Figure 8I, J; arrows). This organisation is quite distinct from that seen in the BIL samples where no bow region was observed (Figure 2).

In the CZ of regenerating lenses, both ZO-1 and γ-tubulin staining was observed in between the two layers of LECs on day 1 after surgery (Figure 9A, B) and this pattern of staining remained unchanged at all time-points studied (Figure 9C, H). N-cadherin is restricted in expression to the cells attached to the posterior lens capsule by day 7 (Figure 9C) and remained so at day 15 and 30 (Figure 9E, G respectively). At the new equator, although the fibre cell organisation and the bow region were not as regular as equatorial regions elsewhere in the regenerating lens, both ZO-1 and γ-tubulin indicated an appropriate EFI had been established (Figure 9I-L).

Organelles degraded at the late stage of lens regeneration

An organelle free zone (Bassnett, 1995, 2002; Kuwabara and Imaizumi, 1974) started to develop between the 30 and 50 day time point. DAPI staining demonstrated condensed/fragmented cell nuclei in fibre cells in the central region (Figure 10A). These nuclear fragments condensed and were TUNEL-positive (Figure 10E-G). Golgi apparatus and endoplasmic reticulum (ER) markers indicated their presence throughout the superficial fibre cells, but they were not detected in the nucleus and there was a clear gradient in signal between these two regions (Figure 10B-D). The development of an organelle-free zone originating from the centre of regenerated lens contrasts the process of refilling the lens capsular bag after surgery, which starts at the lens equator (Figure

10H). It would appear that the lens fibre cells at the centre are the last to complete their elongation, but amongst the first to start the process of organelle removal.

EMT only occurred at the capsulotomy site during lens regeneration

One layer of cells with weak E-/N-cadherin staining was located on the anterior capsule at the capsulotomy site. LECs were also detected on the posterior capsule at the capsulotomy site on day 1 after surgery (Figure 11A, E). The cell polarity of these cells was unclear due to the weak staining of ZO-1 and the random distribution of γ-tubulin (Figure 11E, I). These cells became multi-layered and displayed a spindle-like morphology with elongated nuclei by day 3. Although E-/N-cadherin and β-catenin expression was still present in most cells, cell polarity was lost according to the dramatic reduction in ZO-1 expression and the irregular location of γ-tubulin (Figure 11B, F and J). These integral membrane proteins had disappeared from some cells by day 7 (Figure 11C, G) and were mainly detected in those cells close to the capsule in day 30 samples (Figure 11D, H and L).

Fibronectin and α-SMA were both detected in the regenerating rat lenses. Their expression was restricted, however, to the cell multilayers at the capsulotomy site. Expression of fibronectin was first detected on day 2 (Figure 12A) and quickly increased as seen for day 3 and 7 samples (Figure 12B, C). It remained detectable at the capsulotomy site even in the day 50 samples (Figure 12D). The expression of α-SMA was detected a day later than fibronectin at the capsulotomy site (Day 3; Figure 12F), but then its expression pattern mirrored that of fibronectin (Figure 12G,H).

DISCUSSION

Mammalian Lens Regeneration adapts as it progresses

Lens regeneration has been studied in some detail for mouse (Medvedovic et al., 2006; Shekhawat et al., 2001), rat (Huang and Xie, 2010; Lois et al., 2010) and rabbit (Gwon, 2006; Lin et al., 2016; Tan et al., 2017). Our conclusion from these studies is that lens regeneration is similar, but not identical, to mammalian lens development (Henry and Hamilton, 2018; Liu et al., 2020b). Both are quite different to the regenerative response that leads to SR formation after cataract surgery (Wormstone et al., 2020) and to the LEC response after BIL implantation as reported here (Figure 1, 2; Table 1) and previously (De Keyzer et al., 2008; Tassignon et al., 2019; Tassignon et al., 2002; Werner et al., 2010). There are important histological differences as a result of SR formation compared to lens development and lens regeneration and the two should not be confused (Huang and Xie, 2010).

Our study compared lens regeneration with lens development and has identified some differences in the timing of important events such as fibre cell elongation and organelle removal, as well as confirming the importance of the EFI to both. One major difference is that there is no embryonic lens to provide the cellular cues for elongation and spatial organisation of the secondary fibre cells as would be available during development (Koenig and Gross, 2020). This difference has long been recognised as potentially important (Gwon, 2006) and the inclusion of a biodegradable implant as a surrogate embryonic nucleus improved the functional outcome for the regenerated lens in a rabbit model (Gwon and Gruber, 2010). It appears that fibre cell elongation in the lens regeneration system depends on all the cells located on the posterior lens capsule

completing their elongation phase. This starts with those cells at the periphery and finishes with those at the centre of the regenerating lens. The apical ends of the cells on both the anterior and posterior lens capsule remain intact, preserving a presumptive EFI. This is quite different to the developmental stage of lens vesicle closure where a similar cell-cell contact is only established once the posterior cells in the lens vesicle have elongated to fill that space (Koenig and Gross, 2020). This interaction and formation of the EFI is crucial to lens formation (Logan et al., 2017). Cell organelle loss starts in those fibre cells that have most recently completed their elongation and from the centre outwards as observed during lens development (Rowan et al., 2017). There is still much to learn about the mechanisms involved in fibre cell elongation (Audette et al., 2017). Candidates include CDK1 becoming activated (Chaffee et al., 2014) along with HSF4 (Gao et al., 2017) that initiate organelle removal from the fibre cells. This implies a common trigger and perhaps this is oxygen sensing (Mansergh et al., 2008) given its clear connection with organelle removal (Bassnett and McNulty, 2003; Brennan et al., 2020). We consider this as a *prima fascia* example of how lens cells sense their environment and respond accordingly to initiate the necessary differentiation programmes and adapting conserved developmental pathways to produce a regenerated lens.

In the first 24 hours there is extensive cell proliferation and an overproduction of LECs as a first response to the surgery in our model and also in the human too (Lin et al., 2016). Removal of the lens fibre cells is a trigger for LEC proliferation (Rakic et al., 1997) as seen when LECs are cultured *in vitro* in the capsular bag (Tholozan et al., 2007; Wormstone et al., 1997). This proliferative response underpins the development of posterior capsule opacification (Rakic et al., 2000), which has a regenerative as well as

a fibrotic component (Wormstone et al., 2020). In that regard, it has been noted that the BIL is an effective surgical solution to prevent the fibrotic component of PCO and instead encourage the regenerative response following cataract surgery (De Groot et al., 2005).

In the rat and rabbit lens regeneration models (Gwon, 2006; Lois et al., 2003; Lois et al., 2010), the cell number and organisation is adjusted so that two apposing anterior and posterior cell monolayers are produced and a new EFI established. Such readjustments may be apoptosis-driven as seen in lens development of other vertebrates such as zebrafish (Cole and Ross, 2001). Another difference is that the apical surfaces of the apposing cell layers remain in contact with one another (Figures 5-9). The apical ends of the primary fibre cells only abut the apical surfaces of the anterior LECs once vesicle closure is complete in rat lens development. Amongst vertebrates there is significant variation in eye lens development (Koenig and Gross, 2020) testifying to the inherent plasticity of the lens system. Nevertheless this ability to adapt to change has limits. The challenges presented to the remaining LECs following cataract surgery, are manifest in the nuanced SR formation after either a traditional LIB (Wormstone et al., 2020) or BIL approach (Figure 2). The SR formed in conjunction with the BIL remains largely transparent (Tassignon et al., 2019; Tassignon et al., 2011; Van Looveren et al., 2015) and similar in morphology to the SR formed after conventional LIB cataract surgery (Marcantonio and Vrensen, 1999; Wormstone et al., 2020). This supports our main thesis that LECs respond to a set of important spatial, ECM, cellular and molecular cues that collectively are required to produce a transparent and optically function eye lens (Kumar et al., 2019; Liu et al., 2020a; Lois et al., 2010; McAvoy et al., 2017; Petrova et al., 2020; Vaghefi and Donaldson, 2018). We suggest that the re-establishment of the apical-apical

cell interaction between the lens cells on apposing anterior and posterior surfaces of the lens capsule is a key event as it leads to the re-establishment of the EFI.

Cell-cell connections, mechanical cues and their role in the different regenerative responses by LECs

In the regenerating lens, it is the reinstatement of lens cell polarity that precedes EFI formation. This is evidenced by the γ-tubulin (Dahm et al., 2007; Millar et al., 1997) and cadherin expression patterns (Beebe et al., 2001; Logan et al., 2017), which are re-established during the first 3 days. N-cadherin becomes restricted to the LECs on the posterior lens capsule and to the fibre cells. It is required for regulating the signalling mechanisms needed for fibre cell elongation and de-nucleation (Logan et al., 2017). Mutations in N-cadherin are linked to cataract (Accogli et al., 2019) and the dynamin binding protein (DNMP1) is also linked to inherited cataract, a protein that regulates tight junction formation and the lenticular cytoskeleton (Ansar et al., 2018). E-cadherin is expressed in the LECs located on the anterior lens capsule. Both cadherins are found on the apposing apical surfaces of LECs and fibre cells where we suggest that they form heterotypic adhesion junctions to then ensure the formation and retention of the EFI. Heterotypic cadherin-based adhesions form in response to mechanical signals, that then elicit the association of β-catenin (Labernadie et al., 2017), which is also seen in the regenerating lens (Figures 8, 9). In embryogenesis the formation of the neural crest cells and the neural plate depend upon β-catenin regulation of E- and N-cadherin and their ability to form heterotypic junctions (Rogers et al., 2018). The olfactory epithelium also depends upon the formation of heterotypic cadherin junctions between epithelial cells and the supporting cells for cell mosaic formation (Katsunuma et al., 2016). We suggest that

the regenerating avascular lens is another system where this heterotypic interaction between N- and E-cadherins is important.

The targeted deletion of N-cadherin highlighted both the signalling role via Rac1 and EphaA2 as well as the complementary adhesive role for AQP0 (Logan et al., 2017). We also observed the expression of AQP0 in the LECs located on the posterior capsule and the regenerated fibre cells (Figure 5), but the central role of this water channel protein to the lens circulation model is equally important (Donaldson et al., 2017; Mathias et al., 2007; Vaghefi and Donaldson, 2018) and the properties this endows to the lens system (Cao et al., 2018; Lois et al., 2010). AQP0 localisation is subject to mechanical influences via the zonular tension (Petrova et al., 2020), which translates capsular tension into altered water transport in the lens (Chen et al., 2019) via TRPV channels and PI3K/Akt signalling (Gao et al., 2015). Of course cadherins themselves are fundamental to the integration of tensile forces and the subsequent mechano-transduction of these signals (Charras and Yap, 2018; Yap et al., 2018), via the cytoskeleton (Khalilgharibi et al., 2019), Hippo (Kumar et al., 2019) and for example other signalling pathways (Gunhaga, 2011; McAvoy et al., 2017). Connexins and integrins also integrate these mechano-physical inputs so that lens metabolism and redox potential is also adjusted (Liu et al., 2020a). Any tissue engineering, and especially lens regeneration or surgical approaches to treat cataract have to provide the required mechanobiological inputs and cues (Kim et al., 2021). New methods are being developed to measure the biomechanical characteristics of the lens (Ambekar et al., 2020). Cataract surgery changes capsule tension (Berggren et al., 2021) irrespective of whether this is the BIL or LIB approach. Lens capsule integrity is clearly important to both lens cell organisation and the optical function (Lin et al., 2016;

Lois et al., 2010) as leaving the bag open induces a disorganised regenerative response (Tan et al., 2017). Of course the fact that the IOL will also interrupt lens physiology by disturbing the electrical, water, ion and oxygen gradients that are essential to lens function and its homeostasis is a mute point (Liu et al., 2020a; Lois et al., 2010; Petrova et al., 2020; Shui and Beebe, 2008; Vaghefi and Donaldson, 2018). It remains to be determined how these factors each contribute to the fibre cell organisation in the SR compared to that in the regenerated lens and we suggest that these represent two distinct end points that should not be conflated (Huang and Xie, 2010). The data presented here and by others regarding regeneration in the BIL system (De Keyzer et al., 2008; Werner et al., 2010) show lens cells respond as expected to their local environment. Its comparison with the rat lens model revealed that the first few days after surgery are critical to which of these outcomes will dominate. Our data suggest that the reformation of the EFI interface and the re-establishment of the iconic bow region are a consequence of the retention and sealing of the lens capsule. Collectively these help establish the cues needed for transparency and optical function, but this outcome is not guaranteed (Gwon, 2006; Gwon et al., 1999; Wu et al., 2017). This ultimately reflects our emerging understanding of the complexity of the spatial cellular organisation (Al-Ghoul et al., 2001; Kuszak et al., 1994; Kuszak et al., 2004), the required biomechanical signals and LEC responses (Kim et al., 2021) as well as the physiology and optics (Donaldson et al., 2017; Kalligeraki et al., 2020; Vaghefi and Donaldson, 2018) of the lens.

COMPETING INTERESTS

The authors declare that they have no competing interests.

AUTHORS' CONTRIBUTIONS

The study was conceived by RAQ and NL. The experiments were designed by WW, RAQ, NL and MJ. The experiments were performed by WW. A special cell counting software was written by CS and further statistical analysis was carried out by SR. The manuscript was written by RAQ with contributions from WW, ARP, MJ, NL, SR and MJ. All authors read and approved the final manuscript.

ACKNOWLEDGEMENTS

The financial support of is gratefully acknowledged. We would like to thank Sabrina Chusnul Chotimah in University of Indonesia for helping data analysis and preparation of some samples for confocal microscope study. We also thank Rosie Fordyce in University of Aberdeen and Tim Hawkins in Durham University for their kind technical help. We acknowledge the life science support unit of Durham University for assistance in animal study. This research is supported by Fight for Sight UK (WJW and MJ; Grant #1538/9).

ABBREVIATIONS

aSMA	alpha smooth muscle actin	AQP0	Aquaporin 0
BIL	bag in the lens	CDK1	Cyclin Dependent Kinase 1
CZ	Central Zone of lens epithelium	DAPI	4′,6-diamidino-2-phenylindole
EdU	5-ethynyl-2'-deoxyuridine	EFI	Epithelial Fibre cell Interface
EMT	Epithelial Mesenchymal Transition	HSF4	Heat Shock factor 4
IOL	Intraocular Lens	LECs	lens epithelial cells
LIB	Lens in the bag	PCO	Posterior capsular opacification
PFA	paraformaldehyde	PTM	Post Translational Modification
SR	Soemmerring's Ring	ZO1	Zona Occludens (Tight Junction) Protein 1

FIGURE LEGENDS

Figure 1. Bag in the Lens (BIL) Implants and the response of the retained lens cells to its insertion. A schematic showing the principle of the BIL approach (A), followed by examples from patients (B, C). The schematic (A) illustrates the implantation of the BIL and the intentional sealing of the lens capsule during surgery by locating both the anterior and posterior edges of the capsule rhexes into the BIL to create a sealed environment. Rarely a tension ring is needed to hold the IOL in place, but this is usual in for other IOLs.

(B). Whilst the capsule-contained rim remains largely transparent, Eschnig's Pearls (B, arrow) form after implantation of the BIL and there are regional differences in transparency (arrowheads) suggestive of altered cell organization at these points. The BIL implant remains centred and un-tilted in these slit lamp images. (B) was taken 6 months after implantation.

(C). A Miyake-Apple posterior view of the sample taken for proteomic and histological analysis. The eye was removed 4.5 years after implantation. The lens rim appears opaque as a result of the fixation as noted in previous examples (Werner et al., 2010), but the implanted IOL and cornea are clear and optically functional as seen from the type script. Notice that there are localised density inconsistencies within the lens periphery (arrow).

Figure 2. Characterisation of a BIL sample by light (A) and electron microscopy (B-F).

(A). Section showing the transition in thickness for the anterior (a) and posterior (p) lens capsule. Notice that lens epithelial cells (LECs) are found on both capsule surfaces. The

lens fibre cells (fc) form the bulk of the cells in the section, but in the absence of a distinct bow region these fibre cells appear to lack the organization expected for a lens.

(B). Lens fibre cells (brackets) are seen in longitudinal section, but their width is variable. These fibre cells are distal to other cells nearer to the BIL and it is apparent that the extent of differentiation across the lens rim is variable and some are in the process of degenerating (star). In (C), fiber cells exhibit some of the expected features of differentiation, including ball and socket interdigitations (arrow). These fiber cells are also organelle free, although there are frequent membrane defined features in these cells.

(D) Fibre cell cytoplasm is uniform and the interface between neighboring fibre cells (arrow) shows tight apposition and regularity, a feature required to minimize light scatter. In some regions of the lens rim (E), there is an abundance of vesicular bodies. In (F), two micrographs have been tiled to evidence the disorganization of both the epithelial cell layer and the fibre cells and also the epithelial-fibre cell interface. Fibre cell junctions (bracket) are adjacent to elongating epithelial cells (asterisks) that appear to have limited connection with the lens capsule. Notice the variation in cytoplasmic density and the irregular fibre cell profiles and width.

Scale Bars = 5 μm in all panels except (A) and (F) where they represent 50 μm and 10μm respectively.

Figure 3. Images of newly regenerated lens at different time points following lens extraction. On day 1 postoperatively, the anterior capsule at the capsulotomy site (black arrows) folds back and only the posterior capsule remains here (A). A white scar with some wrinkles around is formed at the capsulotomy site soon after surgery (B and C,

black arrows), while the rest area remains clear and flat. The regeneration is initiated from the periphery of the lens (white arrows) where it is much thicker than the central area on day 15 (D). On day 30 a clear regenerated lens is formed with a three-dimensional structure in the periphery and central area (E). At the capsulotomy site, the regenerated tissue appears to have erupted from the confines of the capsule (E, white arrows). (F). The majority of the regenerated lens remain clear on day 50 but sometimes white opacities (black arrowhead) or cavities (white arrowhead) can be observed. The capsulectomy site was also breached by translucent cell material (arrow). The capsular bags on day 1, 3 and 7 (A-C) have been fixed and several cuts were made in the periphery for efficient EdU labelling.

Figure 4. Cell proliferation detected by EdU labelling in the regenerated lens of different time points. In the flat-mount of control lens, many dividing cells are observed at the equator (outside of the white circle) and some are present in the CZ (inside of the white circle). A burst of cell proliferation is evident by day 1 postoperatively (A) and this decreases fast as seen by the day 2 sample (B). In (C) the change in proliferation indexes over the full 30 day period in the control and post-surgery in the regenerating lens over. Circles depict observed means and shaded regions depict 95% credible intervals. Scale bars = 500 μm.

Figure 5. The lens cell reorganization and fiber cell differentiation at the equator during lens regeneration. Only the monolayer of epithelial cells is left immediately after surgery with E-cadherin expressed in all the cells except those at the end of the TZ (A, white arrows). This single layer of cells becomes multilayered on day 1 (B) and day 2 (C) postoperatively, which reorganize into two layers in most areas on day 3 with continuous

expression of E-Cadherin in all of the cells (D). In those areas still with multilayer of cells at the equator on day 3, many apoptotic cells with highly condensed chromatin or broken nuclei (white arrows) were detected (E). On day 7, E-cadherin expression is restricted to the cells on anterior capsule while AQP0 expression initiates in the elongated cells on the posterior side (F). The regeneration area with cuboidal epithelial cells on the anterior side (E-cadherin) and elongated fiber cells on the posterior side (AQP0) increases at the equator on day 15 (G). The lens fiber cells elongate dramatically and bidirectionally on day 30 (H) and their nuclei progressively shift towards anterior to form a typical lens bow on day 50 (I). Scale bars = 25 μm.

Figure 6. The lens cell organisation and fiber cell differentiation in the CZ and new equator during lens regeneration. E-cadherin shows that cells in the CZ start to form two layers on day 1 postoperatively (A) and retain as two layers on day 3 (B) and day 7 (C). The cell height in the two layers increases equally within the first 7 days. On day 15 (D) and day 30 (E) the cells on posterior side elongate faster and express AQP0 while the anterior cuboidal cells still retain the E-cadherin expression. The new equator is located next to the capsulotomy site (F-I). E-cadherin expression is losing from the cells on the posterior side but AQP0 expression has not started on day 7 (F). On day 15, E-cadherin completely disappears from the elongated posterior cells and it is replaced by AQP0 (G). The new equator shows similar cell organisation as the opposite equator on day 30 and day 50 with the flat epithelial cells (E-cadherin) in the anterior side and the elongated fiber cells (AQP0) in the posterior side (H-I). Scale bars = 25 μm.

Figure 7. Expression of γC-crystallin in different regions of the regenerated lens. γC-crystallin is first detected in the cytoplasm of elongate cells on the posterior side of the

equator on day 7 postoperatively (A-C). Its expression at the equator increases on day 15 (D) and also appears in the elongated cells on the posterior side of the CZ (E) and new equator (F). It is persistently present in the fibre cells of the three regions on day 30 (G-I). Scale bars = 25 μm.

Figure 8. Establishment of cell polarity at the equator of regenerated lenses. The location of ZO-1 and γ-tubulin in the multilayer of cells at the equator is not regular on day 1 postoperatively (A-B). They are restricted to the interface of two layers of cells on day 3 (C-D) and remain there during the following time-points studied (E-J). On day 30 postoperatively, they accumulate in the middle of transitional zone (I-J: arrows) and are absent from the last several elongated cells. N-cadherin is expressed in all the cells of this region on day 1 (A) and day 3 (C) but is only retained in the elongated cells on the posterior side from day 7 to day 30 (E, G and I). Notice that N-cadherin expression is lost from the fibre cells indicated (I, bracket). β-catenin is weakly detected at the plasma membranes of cells on day 1 (B). Its expression increases from day 3 (D) and is present in the cells on both the anterior and posterior lens capsules (F, H and J). The DAPI stain confirms that the lens bow has been re-established (I). Scale bars = 25 μm.

Figure 9. Establishment of cell polarity in the CZ and new equator during lens regeneration. Both ZO-1 and γ-tubulin are present at the interface of the newly formed two layers of flat cells in the CZ on day 1 postoperatively (A-B) and remained there in the following time-points studied (C-H). N-cadherin is weakly expressed in all the cells in this region on day 1 (A). Its expression increases on day 7 and is restricted to the cells attached to the posterior capsule (C). With the proceeding fibre cell differentiation on the posterior side, N-cadherin is only detected in the elongated fiber cells (E and G), but by

day 30 (K), levels are decreasing in the fibre cells at the centre of the lens on the optical axis. Unlike N-cadherin, β-catenin is persistently present in all the cells of the CZ (A-H). At the new equator, ZO-1 and γ-tubulin are also located at the epithelial-fibre interface on day 15 (I-J). They maintain this location on day 30 except that they are absent from the last several elongated cells (K-L). The expression pattern of N-cadherin and β-catenin here is similar to the CZ (I-L). Scale bars = 25 μm.

Figure 10. Degradation of nuclei, Golgi apparatus and endoplasmic reticulum (ER) at the central regenerated lens on day 50 postoperatively. The superficial fibre cell nuclei elongate and shift towards anterior to reform the iconic bow region. The chromatin stained by DAPI condenses and finally disappears in the deep cortex (A). This coincides with the disappearance of Golgi apparatus (B) and ER (C). The condensed chromatin remnants are TUNEL-positive (E-G). Scale bars = 25 μm.

H. A schematic summarizing our observations on lens regeneration in the rat, emphasizing the initiation of fibre cell elongation at the lens periphery and the formation of a new equatorial region adjacent to the capsulotomy site. Data for the equatorial region distal to and flanking the capsulotomy site on the lens capsule were difficult to obtain and we indicate this by annotating this region differently in the schematic.

Figure 11. Loss of lens cell adhesion proteins and cell polarity at the capsulotomy site during lens regeneration. E-cadherin is weakly expressed in the cells located on the curled anterior capsule at the capsulotomy site on day 1 postoperatively (A). Its expression increases on day 3 and is present in most multilayer of cells (B). With the increase of cell layers and elongation of nuclei on day 7 it disappears from many cells (C) and this situation is persistent on day 30 (D). N-cadherin and β-catenin also display similar

changes in the cells of this region (E-I). Weak ZO-1 foci are observed in some cells on day 1 postoperatively (E) but its expression is lost in the multilayer of cells of later time points (F-H). γ-tubulin shows random location in the cells of all time points (I-L). Scale bars = 25 μm.

Figure 12. Expression of fibronectin and α-SMA at the capsulotomy site during lens regeneration. Fibronectin expression is first detected in the multilayered cells at the capsulotomy site on day 2 postoperatively (A) and continues to increase from day 3 (B) to day 7 (C). Fibronectin remains detectable in the day 50 sample (D). α-SMA is not observed in this region on day 2 (E), but is present at day 3 (F). Its expression on day 7 (G) and day 50 (H) is quite similar to fibronectin. Scale bars = 25 μm.

Supplementary Figure 1. Coomassie stained 4-12% (w/v) NuPAGE Bis-Tris gel showing four separate extracts from the BIL sample. Proteomic analysis of the major bands (arrows) confirmed the presence of αA-, αB-, βA4, βB2- and γS-crystallin. M = marker proteins, Page Rule plus pre-stained protein ladder, in order of increasing relative mobility from the top of the gel are, 250, 130, 100, 70, 55, 35, 25, 15, 10 kDa.

Supplementary Figure 2. Frozen section from a day 50 regenerated rat lens probed with AQP0 antibodies to highlight fiber cell membrane profiles in the equatorial and nuclear regions to illustrate the regularity of the fiber cell profile. Sections were counter stained with E-cadherin (red channel) and DAPI (blue channel) to identify the lens epithelium and cell nuclei respectively. Scale bar = 25μm

TABLE 1A. PROTEIN IDENTIFICATION OF FOUR SAMPLES FROM DIFFERENT LOCATIONS OF THE BIL RIM.

A peptide false discovery rate (FDR) set at <1% and requiring 2 unique peptides per protein. Identified products are colour coded; green, present in 3 or more; yellow present in two of the 4 sampled sites. The full dataset will be uploaded to PRIDE database (https://www.ebi.ac.uk/pride/) upon publication.

IDENTIFIER	NAME	H1	H2	H3	H4
Crystallins, chaperones					
P02489|CRYAA_HUMAN	alphaA-crystallin	x	x	x	x
P02511|CRYAB_HUMAN	alphaB-crystallin	x	x	x	x
P04792|HSPB1_HUMAN	HSP27	x	x	x	x
P53674|CRBB1_HUMAN	beteB1-crystallin	x	x	x	x
P43320|CRBB2_HUMAN	betaB2-crystallin	x	x	x	x
P26998|CRBB3_HUMAN	betaB3-crystallin	x	x	x	x
P05813|CRBA1_HUMAN	betaA 1-crystallin	x	x	x	x
P53672|CRBA2_HUMAN	betaA 2-crystallin	x	x	x	x
P53673|CRBA4_HUMAN	betaA 4-crystallin	x	x	x	x
P22914|CRBS_HUMAN	gammaS-crystallin	x	x	x	x
P07320|CRGD_HUMAN	gammaD-crystallin	x		x	x
P08238|HS90_HUMAN	HSP90A and 90B identical		x		x
Calcium and Iron binding proteins					
Q13938|CAYP1_HUMAN	Calcyphosin	x	x	x	x
P26447|S10A4_HUMAN	Protein S100-A4		x	x	
P02792|FRIL_HUMAN	Ferritin light chain		x	x	
Cytoskeleton – actin and intermediate filaments					
P08670|VIME_HUMAN	Vimentin	x	x	x	x
Q12934|BFSP1_HUMAN	Beaded filament structural protein 1; filensin	x	x	x	x
Q13515|BFSP2_HUMAN	Beaded filament structural protein 2; CP49	x	x	x	x
P58546|MTPN_HUMAN	Myotrophin	x	x	x	x
P60709|ACTB_HUMAN	B- or G-Actin	x	x	x	x
Q13813|SPTN1_HUMAN	Spectrin alpha chain	x	x	x	x
Q01082|SPTB2_HUMAN	Fodrin: Spectrin beta chain			x	x
P62328|TYB4_HUMAN	Thymosin beta-4	x		x	
P23528|COF1_HUMAN	Cofilin	x		x	
P07437|TBB5_HUMAN	Tubulin beta		x	x	
O75781|PALM_HUMAN	paralemmin-1	x		x	
Q14019|COTL1_HUMAN	Coactosin-like protein	x	x		
Glycolytic Enzymes/carbohydrate metabolism					
P06733|ENOA_HUMAN	Enolase - glycolytic enzyme	x	x	x	x
P60174|TPIS_HUMAN	Triose phosphate isomerase	x	x	x	x
P04406|G3P_HUMAN	GAPDH	x	x	x	x
P09972|ALDOC_HUMAN	Fructose bisphosphate aldolase C	x	x	x	x
P04075|ALDOA_HUMAN	Fructose bisphosphate aldolase A	x	x	x	x
P00558|PGK1_HUMAN	Phosphoglycerate kinase 1	x	x	x	x

P14618|KPYM_HUMAN	Pyruvate kinase	x	x	x	x
P00338|LDHA_HUMAN	lactate dehydrogenase	x		x	
Nuclear Proteins and Function/Ribosomal/Golgi					
P62258|1433E_HUMAN	14-3-3 protein epsilon	x	x	x	
Q01469|FABP5_HUMAN	Fatty acid-binding protein 5	x	x	x	x
P62987|RL40_HUMAN	Ubiquitin-60S ribosomal protein L40		x	x	x
P63104|1433Z_HUMAN	14-3-3 protein Zeta/delta		x	x	
Q14974|IMB1_HUMAN	Importin 1		x		x
P62805|H4_HUMAN	Histone H4	x			x
Extracellular Matrix and Membrane Components					
P30086|PEBP1_HUMAN	Phosphatidylethanolamine-binding protein 1	x	x	x	x
P09382|LEG1_HUMAN	Galectin 1	x	x	x	x
P35555|FBN1_HUMAN	Fibrillin-1	x	x	x	x
P62937|PPIA_HUMAN	Peptidyl-prolyl cis-trans isomerase A	x	x	x	x
P08572|CO4A2_HUMAN	TypeIV collagen alpha2 chain	x	x		
P07108|ACBP_HUMAN	Acyl-CoA-binding protein		x	x	
P35237|SPB6_HUMAN	Serpin B6		x		x
P01009|A1AT_HUMAN	Alpha-1-antitrypsin	x		x	
Oxidative Stress Defence					
P16152|CBR1_HUMAN	Carbonyl reductase	x	x	x	x
Q99497|PARK7_HUMAN	Parkinson disease protein 7	x	x	x	x
Q06830|PRDX1_HUMAN	Peroxiredoxin-1	x	x	x	x
P30041|PRDX6_HUMAN	Peroxiredoxin-6	x	x	x	x
P00352|AL1A1_HUMAN	Retinal dehydrogenase 1	x		x	x
P48637|GSHB_HUMAN	Glutathione synthetase	x	x		x
P00441|SODC_HUMAN	SOD1		x	x	
Proteolysis/Ubiquitin Degradation pathway					
P09936|UCHL1_HUMAN	Ubiquitin C-terminal hydrolase isozyme L1		x	x	x
P0CG47|UBB_HUMAN	Polyubiquitin B		x	x	x

TABLE 1B. ACETYLATION, DEAMIDATION AND OXIDATION MODIFICATIONS OF THE THE MAJOR CRYSTALLIN AND CYTOSKELETAL PROTEINS DETECTED IN THE BIL SAMPLE.

Identified products are colour coded; green, present in 3 or more of the sampled regions; yellow present in two of the 4 sampled sites. Acetylation of CRYAA and CRYAB has been previously reported (Hains and Truscott, 2007; Nagaraj et al., 2012). Oxidation of M138 has been reported As too has the deamidation of N6, N90, N147 in CRYAA (Hains and Truscott, 2007, 2010; Lund et al., 1996) and N108,N151 The γS-crystallin deamidation sites for both aging and cataract samples evidenced N92 and N192 (Hooi et al., 2012), but here we report N15 is also deamidated in the BIL sample. Some previously unreported modifications are indicated (pink), but we point out these data are qualitative and not quantitative. The full dataset will be uploaded to PRIDE database (https://www.ebi.ac.uk/pride/) upon publication.

Protein	HS 1	HS 2	HS 3	HS 4
P02489|CRYAA_HUMAN				
Acetylation M1* M(+42.01)DVTIQH	+	+	+	+
Acetylation S66 S(+42.01)DRDK		+		+
Acetylation V89 V(+42.01)QDDFVE		+	+	+
Acetylation Q104 Q(+42.01)DDHGY		+		+
Acetylation I146 I(+42.01)QTGLD	+	+	+	+
Deamidation Q6* VTIQ(+.98)HPW	+	+	+	+
Deamidation Q90* VQ(+.98)DDFVE	+		+	+
Deamidation Q147* IQ(+.98)TGLDA	+	+	+	+
Oxidation M1 M(+15.99)(+42.01)DVTI	+	+	+	+
Oxidation H7 TIQH(+15.99)P	+	+	+	+
Oxidation W9 QHPW(+15.99)FK	+	+	+	+
Oxidation M138 ADGM(+15.99)LTF	+		+	
Oxidation H154 LDATH(+15.99)AE	+		+	+
P02511|CRYAB_HUMAN				
Acetylation M1* M(+42.01)DIAIH	+	+	+	+
Acetylation P130 P(+42.01)LTITSSLSS		+	+	
Deamidation N78 FSVN(+.98)LDV	+		+	+
Deamidation N146 LTVN(+.98)GPRK.			+	+
Oxidation M1 M(+15.99)(+42.01)DIAIH	+	+	+	+
Oxidation H7 DIAIHH (+15.99)	+	+		+
Oxidation W9 IHHPW(+15.99)	+	+	+	+
Oxidation W60 APSW(+15.99)FDT	+	+	+	+
Oxidation M68 GLSEM(+15.99)RLEC	+	+	+	+
Oxidation H83 H(+15.99)FSPEEL		+		+
Oxidation H101 VIEVH(+15.99)GK	+			+
P04792|HSPB1_HUMAN				
Acetylation L28 L(+42.01)FDQA		+		+
Acetylation Q80 Q(+42.01)LSSGVS		+	+	
Acetylation L172 L(+42.01)ATQS		+	+	+
Deamidation Q80 Q(+.98)LSSGV			+	+

Deamidation N102 LDVN(+.98)HFAP			+	+
Deamidation N177 QSN(+.98)EITI	+	+	+	+
P53672|CRBA2_HUMAN				
Acetylation S2 S(+42.01)SAPA	+	+	+	+
P53673|CRBA4_HUMAN				
Acetylation L107 L(+42.01)TIFEQE		+	+	+
Acetylation S181 G.S(+42.01)HAPT		+	+	
Deamidation Q23 DEDGFQ(+.98)G		+		+
Deamidation N114 TIFEQEN(+.98)F		+	+	+
Oxidation M14 M(+15.99)VVWDE	+	+	+	+
P53674|CRBB1_HUMAN				
Acetylation A7 A(+42.01)SASATV		+	+	
P43320|CRBB2_HUMAN				
Acetylation A2 A(+42.01)SDHQT	+	+	+	+
Acetylation W82 W(+42.01)DSWTS		+	+	+
Acetylation 109 I(+42.01)ILYENP			+	+
Acetylation D173 D(+42.01)SSDFG		+	+	
Acetylation S174 S(+42.01)SDFGA	+	+	+	+
Deamidation Q8 DHQ(+.98)TQAG	+	+	+	+
Deamidation N116 ENPN(+.98)FTG	+	+	+	+
Deamidation Q147 VQ(+.98)SGTWVG	+	+	+	
Oxidation W85 WDSW(+15.99)TSSR	+		+	+
Oxidation M122 M(+15.99)EIIDDDVP		+	+	
Oxidation W151 GTW(+15.99)VGYQ	+		+	+
P26998|CRBB3_HUMAN				
Deamidation N155 AIN(+.98)GTWVG		+		+
P22914|CRBS_HUMAN				
Deamidation N15 YEDKN(+.98)FQGR		+	+	+
Deamidation Q93 PSGGQ(+.98)YK	+	+	+	+
P08670|VIME_HUMAN				
Oxidation M154 YEEEM(+15.99)R.	+		+	
Oxidation M183 LAEDIM(+15.99)R	+		+	
Oxidation M391 M(+15.99)ALDIE	+		+	
P60709|ACTB_HUMAN				
Oxidation M190 DYLM(+15.99)K	+	+	+	+
Oxidation M325 LAPSTM(+15.99)K	+	+		+

SUPPLEMENTARY MATERIALS

The detail of the statistical model is presented in this section along with the raw data used to construct the model.

REFERENCES

Accogli, A., Calabretta, S., St-Onge, J., Boudrahem-Addour, N., Dionne-Laporte, A., Joset, P., Azzarello-Burri, S., Rauch, A., Krier, J., Fieg, E., Pallais, J.C., McConkie-Rosell, A., McDonald, M., Freedman, S.F., Rivière, J.B., Lafond-Lapalme, J., Simpson, B.N., Hopkin, R.J., Trimouille, A., Van-Gils, J., Begtrup, A., McWalter, K., Delphine, H., Keren, B., Genevieve, D., Argilli, E., Sherr, E.H., Severino, M., Rouleau, G.A., Yam, P.T., Charron, F., Srour, M., 2019. De Novo Pathogenic Variants in N-cadherin Cause a Syndromic Neurodevelopmental Disorder with Corpus Collosum, Axon, Cardiac, Ocular, and Genital Defects. Am J Hum Genet 105, 854-868.

Al-Ghoul, K.J., Nordgren, R.K., Kuszak, A.J., Freel, C.D., Costello, M.J., Kuszak, J.R., 2001. Structural evidence of human nuclear fiber compaction as a function of ageing and cataractogenesis. Exp Eye Res 72, 199-214.

Alon, R., Assia, E.I., Kleinmann, G., 2014. Prevention of posterior capsule opacification by an intracapsular open capsule device. Invest Ophthalmol Vis Sci 55, 4005-4013.

Ambekar, Y.S., Singh, M., Zhang, J., Nair, A., Aglyamov, S.R., Scarcelli, G., Larin, K.V., 2020. Multimodal quantitative optical elastography of the crystalline lens with optical coherence elastography and Brillouin microscopy. Biomed Opt Express 11, 2041-2051.

Ansar, M., Chung, H.L., Taylor, R.L., Nazir, A., Imtiaz, S., Sarwar, M.T., Manousopoulou, A., Makrythanasis, P., Saeed, S., Falconnet, E., Guipponi, M., Pournaras, C.J., Ansari, M.A., Ranza, E., Santoni, F.A., Ahmed, J., Shah, I., Gul, K., Black, G.C., Bellen, H.J., Antonarakis, S.E., 2018. Bi-allelic Loss-of-Function Variants in DNMBP Cause Infantile Cataracts. Am J Hum Genet 103, 568-578.

Apple, D.J., Lim, E.S., Morgan, R.C., Tsai, J.C., Gwin, T.D., Brown, S.J., Carlson, A.N., 1990. Preparation and study of human eyes obtained postmortem with the Miyake posterior photographic technique. Ophthalmology 97, 810-816.

Audette, D.S., Scheiblin, D.A., Duncan, M.K., 2017. The molecular mechanisms underlying lens fiber elongation. Exp Eye Res 156, 41-49.

Bassnett, S., 1995. The fate of the golgi apparatus and endoplasmic reticulum during lens fibre cell differentiation. Invest Ophthalmol Vis Sci 36, 1793-1803.

Bassnett, S., 2002. Lens organelle degradation. Exp Eye Res 74, 1-6.

Bassnett, S., McNulty, R., 2003. The effect of elevated intraocular oxygen on organelle degradation in the embryonic chicken lens. J Exp Biol 206, 4353-4361.

Beebe, D.C., Vasiliev, O., Guo, J., Shui, Y.B., Bassnett, S., 2001. Changes in adhesion complexes define stages in the differentiation of lens fiber cells. Invest Ophthalmol Vis Sci 42, 727-734.

Berggren, C.C., Ameku, K.A., Pedrigi, R.M., 2021. Altered stress field of the human lens capsule after cataract surgery. J Biomech 115, 110127.

Brennan, L., Disatham, J., Kantorow, M., 2020. Hypoxia regulates the degradation of non-nuclear organelles during lens differentiation through activation of HIF1a. Exp Eye Res 198, 108129.

Burd, H.J., Montenegro, G.A., Panilla Cortés, L., Barraquer, R.I., Michael, R., 2017. Equatorial wrinkles in the human lens capsule. Exp Eye Res 159, 77-86.

Cao, L., Liu, J., Pu, J., Collinson, J.M., Forrester, J.V., McCaig, C.D., 2018. Endogenous bioelectric currents promote differentiation of the mammalian lens. J Cell Physiol 233, 2202-2212.

Chaffee, B.R., Shang, F., Chang, M.L., Clement, T.M., Eddy, E.M., Wagner, B.D., Nakahara, M., Nagata, S., Robinson, M.L., Taylor, A., 2014. Nuclear removal during terminal lens fiber cell differentiation requires CDK1 activity: appropriating mitosis-related nuclear disassembly. Development 141, 3388-3398.

Charras, G., Yap, A.S., 2018. Tensile Forces and Mechanotransduction at Cell-Cell Junctions. Curr Biol 28, R445-r457.
Chen, Y., Gao, J., Li, L., Sellitto, C., Mathias, R.T., Donaldson, P.J., White, T.W., 2019. The Ciliary Muscle and Zonules of Zinn Modulate Lens Intracellular Hydrostatic Pressure Through Transient Receptor Potential Vanilloid Channels. Invest Ophthalmol Vis Sci 60, 4416-4424.
Cole, L.K., Ross, L.S., 2001. Apoptosis in the developing zebrafish embryo. Dev Biol 240, 123-142.
Coscia, F., Doll, S., Bech, J.M., Schweizer, L., Mund, A., Lengyel, E., Lindebjerg, J., Madsen, G.I., Moreira, J.M., Mann, M., 2020. A streamlined mass spectrometry-based proteomics workflow for large-scale FFPE tissue analysis. J Pathol 251, 100-112.
Dahm, R., Procter, J.E., Ireland, M.E., Lo, W.K., Mogensen, M.M., Quinlan, R.A., Prescott, A.R., 2007. Reorganization of centrosomal marker proteins coincides with epithelial cell differentiation in the vertebrate lens. Exp Eye Res 85, 696-713.
De Groot, V., Tassignon, M.J., Vrensen, G.F., 2005. Effect of bag-in-the-lens implantation on posterior capsule opacification in human donor eyes and rabbit eyes. Journal of cataract and refractive surgery 31, 398-405.
De Keyzer, K., Leysen, I., Timmermans, J.P., Tassignon, M.J., 2008. Lens epithelial cells in an in vitro capsular bag model: lens-in-the-bag versus bag-in-the-lens technique. Journal of cataract and refractive surgery 34, 687-695.
DiMauro, M.A., Nandi, S.K., Raghavan, C.T., Kar, R.K., Wang, B., Bhunia, A., Nagaraj, R.H., Biswas, A., 2014. Acetylation of Gly1 and Lys2 promotes aggregation of human γD-crystallin. Biochemistry 53, 7269-7282.
Donaldson, P.J., Grey, A.C., Maceo Heilman, B., Lim, J.C., Vaghefi, E., 2017. The physiological optics of the lens. Prog Retin Eye Res 56, e1-e24.
Freel, C.D., al-Ghoul, K.J., Kuszak, J.R., Costello, M.J., 2003. Analysis of nuclear fiber cell compaction in transparent and cataractous diabetic human lenses by scanning electron microscopy. BMC Ophthalmol 3, 1.
Gao, J., Sun, X., White, T.W., Delamere, N.A., Mathias, R.T., 2015. Feedback Regulation of Intracellular Hydrostatic Pressure in Surface Cells of the Lens. Biophys J 109, 1830-1839.
Gao, M., Huang, Y., Wang, L., Huang, M., Liu, F., Liao, S., Yu, S., Lu, Z., Han, S., Hu, X., Qu, Z., Liu, X., Assefa Yimer, T., Yang, L., Tang, Z., Li, D.W., Liu, M., 2017. HSF4 regulates lens fiber cell differentiation by activating p53 and its downstream regulators. Cell death & disease 8, e3082.
Gunhaga, L., 2011. The lens: a classical model of embryonic induction providing new insights into cell determination in early development. Philos Trans R Soc Lond B Biol Sci 366, 1193-1203.
Gwon, A., 2006. Lens regeneration in mammals: a review. Surv Ophthalmol 51, 51-62.
Gwon, A., Gruber, L., 2010. Engineering the crystalline lens with a biodegradable or non-degradable scaffold. Exp Eye Res 91, 220-228.
Gwon, A., Kuszak, J., Gruber, L.J., 1999. Intralenticular implant study in pigmented rabbits: opacity lensmeter assessment. Journal of cataract and refractive surgery 25, 268-277.
Hains, P.G., Truscott, R.J., 2007. Post-translational modifications in the nuclear region of young, aged, and cataract human lenses. J Proteome Res 6, 3935-3943.
Hains, P.G., Truscott, R.J., 2010. Age-dependent deamidation of lifelong proteins in the human lens. Invest Ophthalmol Vis Sci 51, 3107-3114.
Henry, J.J., Hamilton, P.W., 2018. Diverse Evolutionary Origins and Mechanisms of Lens Regeneration. Mol Biol Evol 35, 1563-1575.
Hooi, M.Y., Raftery, M.J., Truscott, R.J., 2012. Age-dependent deamidation of glutamine residues in human γS crystallin: deamidation and unstructured regions. Protein Sci 21, 1074-1079.

Huang, Y., Xie, L., 2010. Expression of transcription factors and crystallin proteins during rat lens regeneration. Mol Vis 16, 341-352.
Kalligeraki, A.A., Isted, A., Jarrin, M., Uwineza, A., Pal, R., Saunter, C.D., Girkin, J.M., Obara, B., Quinlan, R.A., 2020. Three-dimensional data capture and analysis of intact eye lenses evidences emmetropia-associated changes in epithelial cell organization. Sci Rep 10, 16898.
Kappelhof, J.P., Vrensen, G.F., Vester, C.A., Pameyer, J.H., de Jong, P.T., Willekens, B.L., 1985. The ring of Soemmerring in the rabbit: A scanning electron microscopic study. Graefes Arch Clin Exp Ophthalmol 223, 111-120.
Katsunuma, S., Honda, H., Shinoda, T., Ishimoto, Y., Miyata, T., Kiyonari, H., Abe, T., Nibu, K., Takai, Y., Togashi, H., 2016. Synergistic action of nectins and cadherins generates the mosaic cellular pattern of the olfactory epithelium. J Cell Biol 212, 561-575.
Khalilgharibi, N., Fouchard, J., Asadipour, N., Barrientos, R., Duda, M., Bonfanti, A., Yonis, A., Harris, A., Mosaffa, P., Fujita, Y., Kabla, A., Mao, Y., Baum, B., Muñoz, J.J., Miodownik, M., Charras, G., 2019. Stress relaxation in epithelial monolayers is controlled by the actomyosin cortex. Nat Phys 15, 839-847.
Kim, S., Uroz, M., Bays, J.L., Chen, C.S., 2021. Harnessing Mechanobiology for Tissue Engineering. Developmental cell 56, 180-191.
Koenig, K.M., Gross, J.M., 2020. Evolution and development of complex eyes: a celebration of diversity. Development 147.
Kumar, B., Chandler, H.L., Plageman, T., Reilly, M.A., 2019. Lens Stretching Modulates Lens Epithelial Cell Proliferation via YAP Regulation. Invest Ophthalmol Vis Sci 60, 3920-3929.
Kuszak, J.R., Peterson, K.L., Sivak, J.G., Herbert, K.L., 1994. The interrelationship of lens anatomy and optical quality. II. Primate lenses. Exp Eye Res 59, 521-535.
Kuszak, J.R., Zoltoski, R.K., Sivertson, C., 2004. Fibre cell organization in crystalline lenses. Exp Eye Res 78, 673-687.
Kuwabara, T., Imaizumi, M., 1974. Denucleation process in the lens. Invest Ophtahlmol Vis Sci 13, 973-981.
Labernadie, A., Kato, T., Brugués, A., Serra-Picamal, X., Derzsi, S., Arwert, E., Weston, A., González-Tarragó, V., Elosegui-Artola, A., Albertazzi, L., Alcaraz, J., Roca-Cusachs, P., Sahai, E., Trepat, X., 2017. A mechanically active heterotypic E-cadherin/N-cadherin adhesion enables fibroblasts to drive cancer cell invasion. Nat Cell Biol 19, 224-237.
Lampi, K.J., Wilmarth, P.A., Murray, M.R., David, L.L., 2014. Lens beta-crystallins: the role of deamidation and related modifications in aging and cataract. Prog Biophys Mol Biol 115, 21-31.
Lin, H., Ouyang, H., Zhu, J., Huang, S., Liu, Z., Chen, S., Cao, G., Li, G., Signer, R.A., Xu, Y., Chung, C., Zhang, Y., Lin, D., Patel, S., Wu, F., Cai, H., Hou, J., Wen, C., Jafari, M., Liu, X., Luo, L., Zhu, J., Qiu, A., Hou, R., Chen, B., Chen, J., Granet, D., Heichel, C., Shang, F., Li, X., Krawczyk, M., Skowronska-Krawczyk, D., Wang, Y., Shi, W., Chen, D., Zhong, Z., Zhong, S., Zhang, L., Chen, S., Morrison, S.J., Maas, R.L., Zhang, K., Liu, Y., 2016. Lens regeneration using endogenous stem cells with gain of visual function. Nature 531, 323-328.
Liu, C.S., Wormstone, I.M., Duncan, G., Marcantonio, J.M., Webb, S.F., Davies, P.D., 1996. A study of human lens cell growth in vitro. A model for posterior capsule opacification. Invest Ophthalmol Vis Sci 37, 906-914.
Liu, J., Riquelme, M.A., Li, Z., Li, Y., Tong, Y., Quan, Y., Pei, C., Gu, S., Jiang, J.X., 2020a. Mechanosensitive collaboration between integrins and connexins allows nutrient and antioxidant transport into the lens. J Cell Biol 219.
Liu, Z., Wang, R., Lin, H., Liu, Y., 2020b. Lens regeneration in humans: using regenerative potential for tissue repairing. Ann Transl Med 8, 1544.

Logan, C.M., Rajakaruna, S., Bowen, C., Radice, G.L., Robinson, M.L., Menko, A.S., 2017. N-cadherin regulates signaling mechanisms required for lens fiber cell elongation and lens morphogenesis. Dev Biol 428, 118-134.
Lois, N., Dawson, R., McKinnon, A.D., Forrester, J.V., 2003. A new model of posterior capsule opacification in rodents. Invest Ophthalmol Vis Sci 44, 3450-3457.
Lois, N., Reid, B., Song, B., Zhao, M., Forrester, J., McCaig, C., 2010. Electric currents and lens regeneration in the rat. Exp Eye Res 90, 316-323.
Lund, A.L., Smith, J.B., Smith, D.L., 1996. Modifications of the water-insoluble human lens alpha-crystallins. Exp Eye Res 63, 661-672.
Mansergh, F.C., Hunter, S.M., Geatrell, J.C., Jarrin, M., Powell, K., Evans, M.J., Wride, M.A., 2008. Developmentally regulated expression of hemoglobin subunits in avascular tissues. Int J Dev Biol 52, 873-886.
Marcantonio, J.M., Vrensen, G.F., 1999. Cell biology of posterior capsular opacification. Eye (Lond) 13 (Pt 3b), 484-488.
Mathias, R.T., Kistler, J., Donaldson, P., 2007. The Lens Circulation. J Membr Biol.
McAvoy, J.W., Dawes, L.J., Sugiyama, Y., Lovicu, F.J., 2017. Intrinsic and extrinsic regulatory mechanisms are required to form and maintain a lens of the correct size and shape. Exp Eye Res 156, 34-40.
Medvedovic, M., Tomlinson, C.R., Call, M.K., Grogg, M., Tsonis, P.A., 2006. Gene expression and discovery during lens regeneration in mouse: regulation of epithelial to mesenchymal transition and lens differentiation. Mol Vis 12, 422-440.
Millar, A., Hooper, A., Copeland, L., Cummings, F., Prescott, A.R., 1997. Reorganisation of the microtubule cytoskeleton and centrosomal loss during lens fibre cell differentiation. Nova Acta Leopoldiana 299, 169-183.
Nagaraj, R.H., Nahomi, R.B., Shanthakumar, S., Linetsky, M., Padmanabha, S., Pasupuleti, N., Wang, B., Santhoshkumar, P., Panda, A.K., Biswas, A., 2012. Acetylation of αA-crystallin in the human lens: effects on structure and chaperone function. Biochim Biophys Acta 1822, 120-129.
Ong, M.D., Payne, D.M., Garner, M.H., 2003. Differential protein expression in lens epithelial whole-mounts and lens epithelial cell cultures. Exp Eye Res 77, 35-49.
Packard, R., 2019. The Evolution of the Anterior Capsulotomy, in: Tassignon M-J., N.D.S., van Os L., (Ed.), Innovative Implantation Technique. Springer International Publishing, pp. 61-75.
Pande, A., Mokhor, N., Pande, J., 2015. Deamidation of Human γS-Crystallin Increases Attractive Protein Interactions: Implications for Cataract. Biochemistry 54, 4890-4899.
Petrova, R.S., Bavana, N., Zhao, R., Schey, K.L., Donaldson, P.J., 2020. Changes to Zonular Tension Alters the Subcellular Distribution of AQP5 in Regions of Influx and Efflux of Water in the Rat Lens. Invest Ophthalmol Vis Sci 61, 36.
Pigaga, V., Quinlan, R.A., 2006. Lenticular chaperones suppress the aggregation of the cataract-causing mutant T5P gamma C-crystallin. Experimental Cell Research 312, 51-62.
Rakic, J.M., Galand, A., Vrensen, G.F., 1997. Separation of fibres from the capsule enhances mitotic activity of human lens epithelium. Exp Eye Res 64, 67-72.
Rakic, J.M., Galand, A., Vrensen, G.F., 2000. Lens epithelial cell proliferation in human posterior capsule opacification specimens. Exp Eye Res 71, 489-494.
Rappsilber, J., Mann, M., Ishihama, Y., 2007. Protocol for micro-purification, enrichment, pre-fractionation and storage of peptides for proteomics using StageTips. Nature protocols 2, 1896-1906.
Ray, N.J., Hall, D., Carver, J.A., 2017. A structural and functional study of Gln147 deamidation in αA-crystallin, a site of modification in human cataract. Exp Eye Res 161, 163-173.
Rogers, C.D., Sorrells, L.K., Bronner, M.E., 2018. A catenin-dependent balance between N-cadherin and E-cadherin controls neuroectodermal cell fate choices. Mech Dev 152, 44-56.

Rowan, S., Chang, M.L., Reznikov, N., Taylor, A., 2017. Disassembly of the lens fiber cell nucleus to create a clear lens: The p27 descent. Exp Eye Res 156, 72-78.
Ruan, X., Liu, Z., Luo, L., Liu, Y., 2020. The Structure of the Lens and Its Associations with the Visual Quality. BMJ Open Ophthalmol 5, e000459.
Saika, S., Miyamoto, T., Ishida, I., Tanaka, T., Okada, Y., Nagane, Y., Shirai, K., Ohnishi, Y., 2001. Comparison of Scheimpflug images of posterior capsule opacification and histological findings in rabbits and humans. Journal of cataract and refractive surgery 27, 1088-1092.
Schey, K.L., Wang, Z., Friedrich, M.G., Garland, D.L., Truscott, R.J.W., 2020. Spatiotemporal changes in the human lens proteome: Critical insights into long-lived proteins. Prog Retin Eye Res 76, 100802.
Serebryany, E., King, J.A., 2014. The betagamma-crystallins: native state stability and pathways to aggregation. Prog Biophys Mol Biol 115, 32-41.
Shekhawat, D.S., Jangir, O.P., Prakash, A., Pawan, S., 2001. Lens regeneration in mice under the influence of vitamin A. J Biosci 26, 571-576.
Shui, Y.B., Beebe, D.C., 2008. Age-dependent control of lens growth by hypoxia. Invest Ophthalmol Vis Sci 49, 1023-1029.
Sugiyama, Y., Prescott, A.R., Tholozan, F.M., Ohno, S., Quinlan, R.A., 2008. Expression and localisation of apical junctional complex proteins in lens epithelial cells. Exp Eye Res 87, 64-70.
Tan, X., Liu, Z., Zhu, Y., Chen, C., Huang, S., Chen, B., Lin, Z., Chen, J., Tang, X., Qu, B., Liu, X., Luo, L., Deng, J., Shang, F., Wu, M., Chen, W., Lin, H., Liu, Y., 2017. The Fate of In Situ Lens Regeneration is Determined by Capsulorhexis Size. Curr Mol Med 17, 270-279.
Tassignon, M.-J., Ní Dhubhghaill, S., Van Os, L., 2019. Innovative Implantation Technique. Springer International Publishing.
Tassignon, M.J., De Groot, V., Vrensen, G.F., 2002. Bag-in-the-lens implantation of intraocular lenses. Journal of cataract and refractive surgery 28, 1182-1188.
Tassignon, M.J., Gobin, L., Mathysen, D., Van Looveren, J., De Groot, V., 2011. Clinical outcomes of cataract surgery after bag-in-the-lens intraocular lens implantation following ISO standard 11979-7:2006. Journal of cataract and refractive surgery 37, 2120-2129.
Taylor, V.L., al-Ghoul, K.J., Lane, C.W., Davis, V.A., Kuszak, J.R., Costello, M.J., 1996. Morphology of the normal human lens. Invest Ophthalmol Vis Sci 37, 1396-1410.
Tholozan, F.M., Gribbon, C., Li, Z., Goldberg, M.W., Prescott, A.R., McKie, N., Quinlan, R.A., 2007. FGF-2 release from the lens capsule by MMP-2 maintains lens epithelial cell viability. Mol Biol Cell 18, 4222-4231.
Vaghefi, E., Donaldson, P.J., 2018. The lens internal microcirculation system delivers solutes to the lens core faster than would be predicted by passive diffusion. Am J Physiol Regul Integr Comp Physiol 315, R994-r1002.
van Bree, M.C., van der Meulen, I.J., Franssen, L., Coppens, J.E., Reus, N.J., Zijlmans, B.L., van den Berg, T.J., 2011. Imaging of forward light-scatter by opacified posterior capsules isolated from pseudophakic donor eyes. Invest Ophthalmol Vis Sci 52, 5587-5597.
Van Looveren, J., S, N.D., Godts, D., Bakker, E., De Veuster, I., Mathysen, D.G., Tassignon, M.J., 2015. Pediatric bag-in-the-lens intraocular lens implantation: long-term follow-up. Journal of cataract and refractive surgery 41, 1685-1692.
Van Looveren, J., Van Gerwen, V., Schildermans, K., Laukens, K., Baggerman, G., Tassignon, M.J., 2018. Proteomic analysis of posterior capsular plaques in congenital unilateral cataract. Acta ophthalmologica 96, e963-e969.
Vergara, M.N., Tsissios, G., Del Rio-Tsonis, K., 2018. Lens regeneration: a historical perspective. Int J Dev Biol 62, 351-361.
Werner, L., 2019. Histopathological Aspects of Bag-in-the-Lens Implantation, in: Tassignon M-J., N.D.S., van Os L., (Ed.), Innovative Implantation Technique. Springer International Publishing, pp. 17-23.

Werner, L., Tassignon, M.-J., Gobin, L., Rozema, J., Davis, D., Brubaker, J., 2008. Bag-in-the-lens: first pathological analysis of a human eye obtained postmortem. Journal of cataract and refractive surgery 34, 2163-2165.
Werner, L., Tassignon, M.J., Zaugg, B.E., De Groot, V., Rozema, J., 2010. Clinical and histopathologic evaluation of six human eyes implanted with the bag-in-the-lens. Ophthalmology 117, 55-62.
Wormstone, I.M., Liu, C.S., Rakic, J.M., Marcantonio, J.M., Vrensen, G.F., Duncan, G., 1997. Human lens epithelial cell proliferation in a protein-free medium. Invest Ophthalmol Vis Sci 38, 396-404.
Wormstone, I.M., Wormstone, Y.M., Smith, A.J.O., Eldred, J.A., 2020. Posterior capsule opacification: What's in the bag? Prog Retin Eye Res, 100905.
Wu, J.J., Wu, W., Tholozan, F.M., Saunter, C.D., Girkin, J.M., Quinlan, R.A., 2015. A dimensionless ordered pull-through model of the mammalian lens epithelium evidences scaling across species and explains the age-dependent changes in cell density in the human lens. J R Soc Interface 12, 20150391.
Wu, X., Liu, Z., Zhang, X., Wang, D., Long, E., Wang, J., Li, W., Lai, W., Cao, Q., Hu, K., Chen, W., Lin, H., Liu, Y., 2017. Proteomics analysis and proteogenomic characterization of different physiopathological human lenses. BMC Ophthalmol 17, 253.
Yap, A.S., Duszyc, K., Viasnoff, V., 2018. Mechanosensing and Mechanotransduction at Cell-Cell Junctions. Cold Spring Harbor perspectives in biology 10.